Microwave Inverse Scattering
Project Report

Disha Shur

July – December 2018

Contents

1 Introduction

Imaging using inverse microwave scattering has the potential to reproduce images with high accuracy, using dielectric properties of the scatterer. This makes it suitable for applications involving scanning for malignant tissues. Previously, «give literature review»
This report includes the implementation details and further analysis of some previous work such as [1], [2], [3], [4] and [5]

2 Notation and Framework

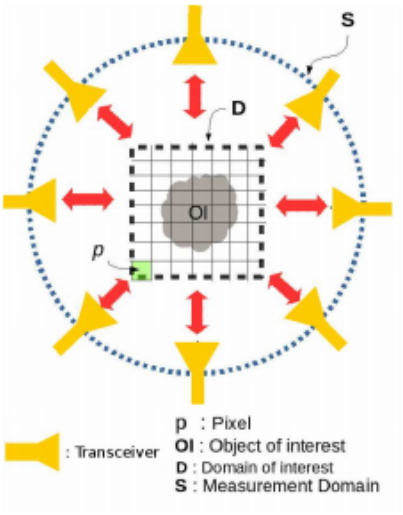

Figure 1: Problem setup [6]

The chief equation governing the scattering problem [7] is as follows:

$$E_z(\vec{r}) = E_z^i(\vec{r}) + \iint_D G(\vec{r}, \vec{r}')\chi(\vec{r}')E_z(\vec{r}')d\vec{r}' \tag{1}$$

where the contrast profile $\chi(\vec{r}')$ is defined as $\chi(\vec{r}') = \epsilon(\vec{r}') - 1$, and $E_z(\vec{r}')$ refers to total electric field at a position $\vec{r}'$. The above equation is valid for all $\vec{r}$, i.e. either for $\vec{r} \in D$ or for $\vec{r} \in S$, where S denotes the domain of measurement points. For purpose of numerical analysis, the imaging domain D is discretized into N square grids, and the internal fields $E_z(\vec{r}')$ and contrast $\chi(\vec{r}')$ are assumed to be constant over each grid. After a suitable evaluation of the integrals in (1) and discretization, we get the following matrix vector relations:

$$\vec{r} \in D: \quad d_v = e_v + G_D\, X\, d_v \tag{2}$$

where, for the v^{th} illumination, $d_v \in \mathbb{C}^{N\times 1}$ represents the total electric filed inside the scatterer, $e_v \in \mathbb{C}^{N\times 1}$ is the incident electric values, $x \in \mathbb{C}^{N\times 1}$ is the dielectric contrast of the object and the matrix $X = \text{diag}(x)$, and $G_D \in \mathbb{C}^{N\times N}$ is a matrix representation of the integral operator in (1) above when $\vec{r}, \vec{r'} \in D$. Similarly, we get

$$\vec{r} \in S: \quad s_v = G_S\, D_v\, x \tag{3}$$

where $s_v \in \mathbb{C}^{M\times 1}$ represents the scattered filed (defined as $E_z(\vec{r}) - E_z^i(\vec{r})$ for $\vec{r} \in S$), the matrix $D_v = \text{diag}(d_v)$, and $G_S \in \mathbb{C}^{M\times N}$ is a matrix representation of the integral operator in (1) above when $\vec{r} \in S, \vec{r'} \in D$.

With the above framework in place, we can define the inverse problem as thus: Estimate the contrast, x, given the incident fields e_v, and noise corrupted scattered field measurements, i.e. $s_v + \zeta$, where ζ represents noise.

3 Born Iterative Method

This section describes the pseudo-code for Born iterative method and discusses the result of the algorithm [1] thus implemented.
The equations used in the development of the algorithm are as described above. Given below are the compact form of the equations.

3.1 Definitions

3.1.1 Object equation

In a compact form, the forward problem, as given in [7], can be written as:

$$\sum_{q=1}^{N} C_{pq} d_{v(q)} = e_{v(p)} \; with \; p = 1, 2, .., N \tag{4}$$

where

$$C_{pq} = \begin{cases} 1 + \frac{j}{2}\chi_p[\pi k a H_1^{(2)}(ka) - 2j] & \text{if } \; p = q \\ \frac{j\pi ka}{2}\chi_q J_1(ka) H_0^{(2)} k\rho_{pq} & \text{if } p \neq q \end{cases}$$

3.1.2 Data equation

In a compact form, the inverse problem, for the v^{th} illumination can be written as:

$$s_{[(v-1)\times M+r]} = G_{S[(v-1)M+r,p]} \times D_{[(v-1)N+p,p]} \times \chi_p, \; p = 1..N, \; r = 1..M, \; v = 1..M \tag{5}$$

where $G_{S[(v-1)\times M+r,p]} = [\frac{-j\pi ka}{2} J_1(ka) H_0^{(2)}(k\rho_{pr})]$

3.1.3 Measures of error

- Relative error:

$$RE = |\frac{s - s_{cal}}{s}| \tag{6}$$

- Contrast error:

$$CE = \frac{||\chi_{recon} - \chi||}{||\chi||} \tag{7}$$

3.2 Algorithm

This section defines the algorithm.

Algorithm 1 Born Iterative Method

procedure BIM(s,χ)
  $d_v \leftarrow e_v$
  while $Convergence \neq True$ **do**

$$\chi \leftarrow [(G_S D)^\dagger (G_S D) + \gamma I]^{-1} (G_S D)^\dagger s$$

▷ Inverse problem

    Update d_v using 4 ▷ Forward problem
    Update s_{cal} using 5
    Update relative error (RE) using 6
    if $RE < threshold$ **then**
      $Convergence = True$
    else
      $Convergence = False$
  return χ_{recon} ▷ Reconstructed contrast

Here, $A^\dagger$ denotes the hermitian of A and threshold is empirically chosen.

3.3 Results

Figure 2 and 3 show the reconstruction of a rectangular dielectric of size $\lambda/2 \times \lambda/3$ with $\chi = 0.1$ at $frequency = 10Ghz$. The forward discretization for the original block was kept at$\lambda/30$ and inverse discretization as mentioned. The reconstructed value of contrast for $\gamma = 10^2$ was found to be erroneous. Figure 4 shows the reconstruction to be better (with low relative and contrast error) for a certain set of γ. Figure 5 shows the variation of relative error with iterations for the object in figure 1.

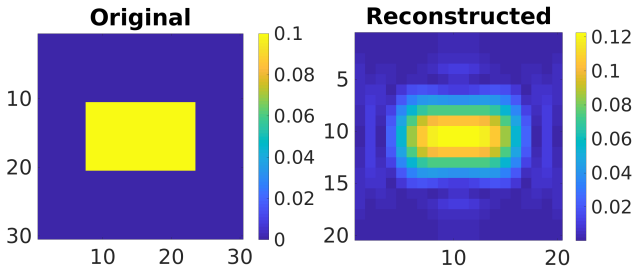

Figure 2: $\chi = 0.1$, $Discretization = \lambda/20$, $\gamma = 10^{-4}$

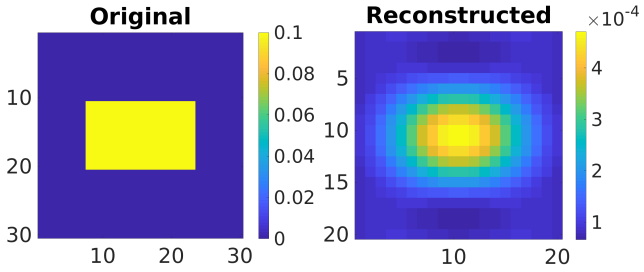

Figure 3: $\chi = 0.1$, $Discretization = \lambda/20$, $\gamma = 10^2$

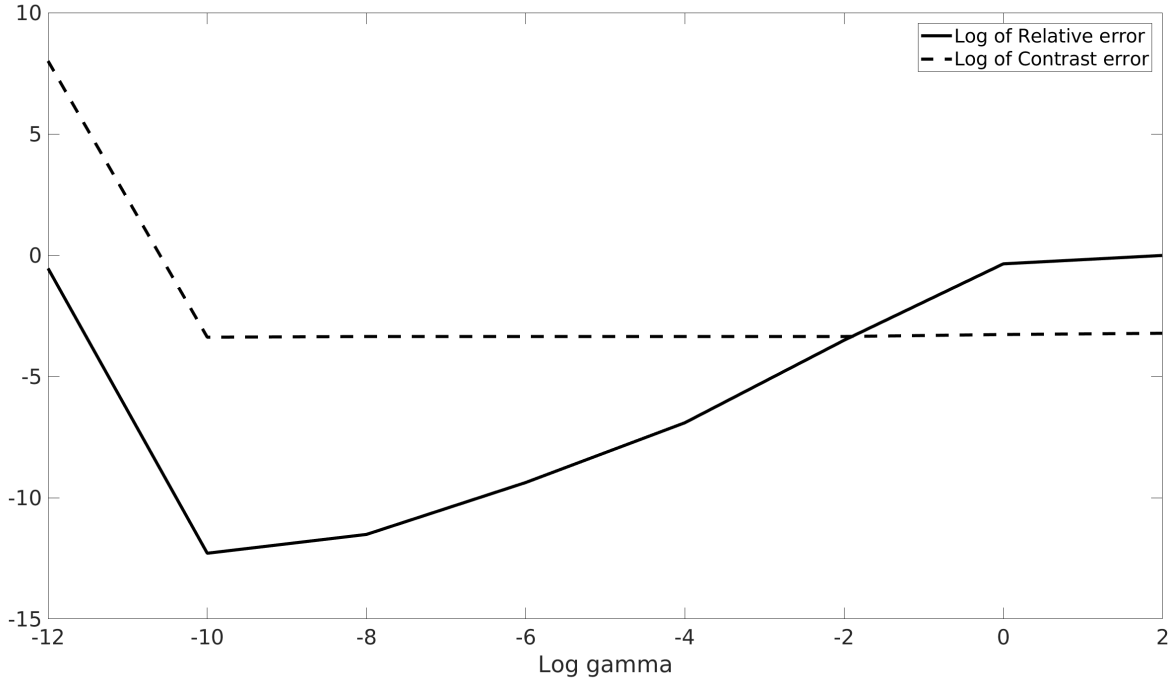

Figure 4: Variation of Relative error and contrast with γ

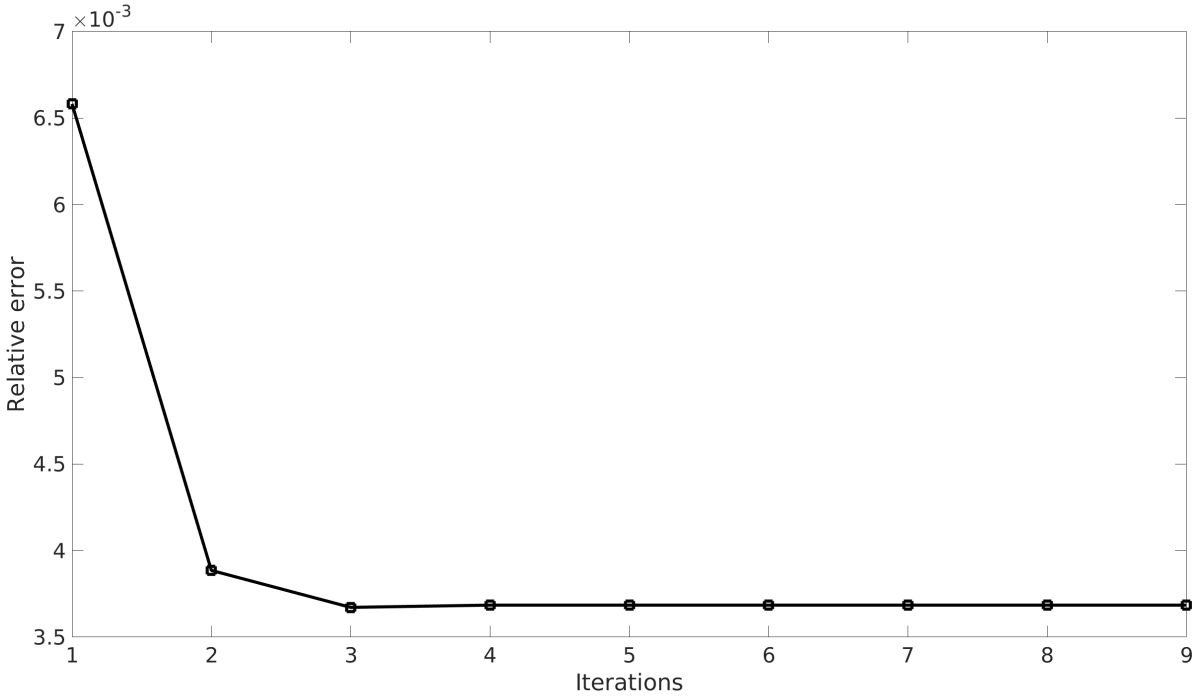

Figure 5: Variation of Relative error with iterations

Figure 6 shows the reconstruction of a sin-like distribution with parameters taken from [2] (with a maximum $\chi = 0.8$ and $radius = 0.5\lambda$ and $frequency = 100Mhz$). The forward discretization for the original block was kept at$\lambda/30$ and inverse discretization at $\lambda/20$. Figure 7 shows the variation of relative error with iterations for the same object.

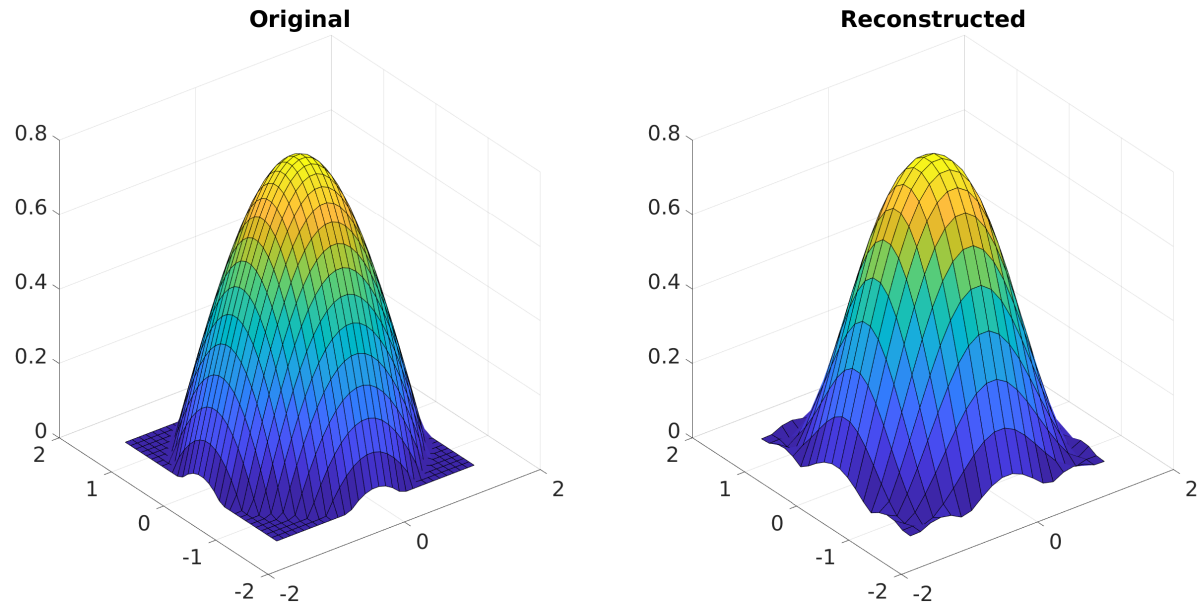

Figure 6: Sin-like distribution with $\chi = 0.8$ and $frequency = 100Mhz$

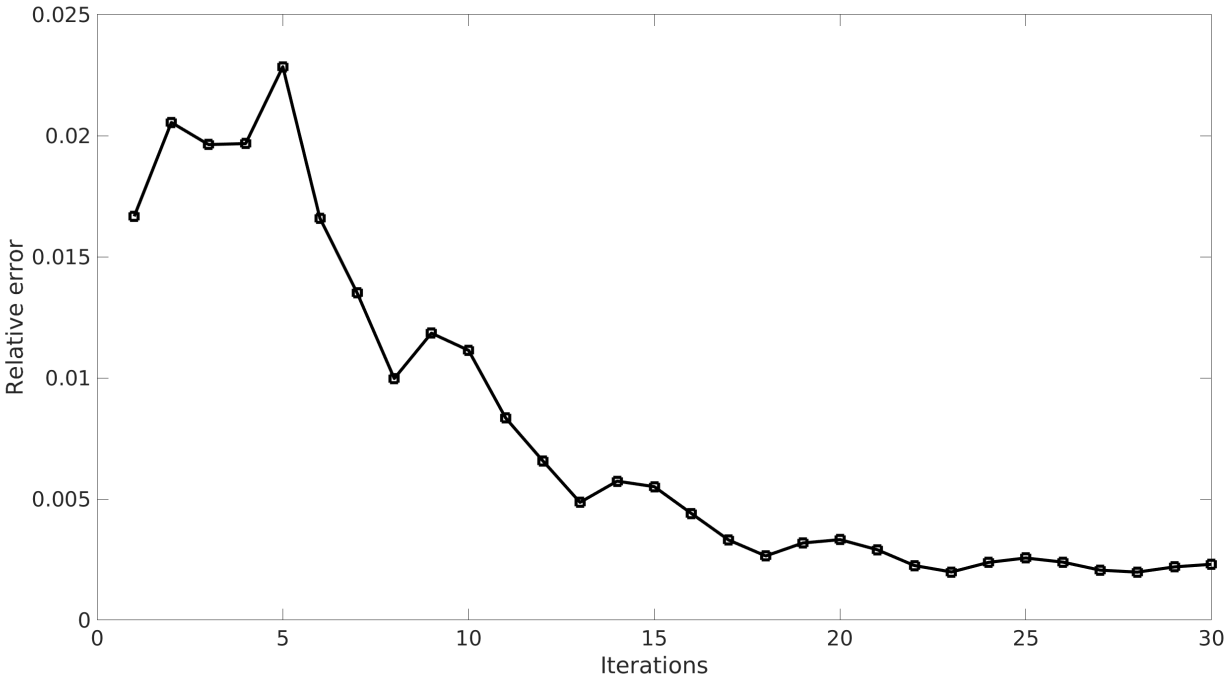

Figure 7: Variation of Relative error with iterations for sin-like distribution

Figures 8 and 9 show the results on using SVD for finding the solution. SVD was calculated for all the transmitters together and not for each transmitter individually.

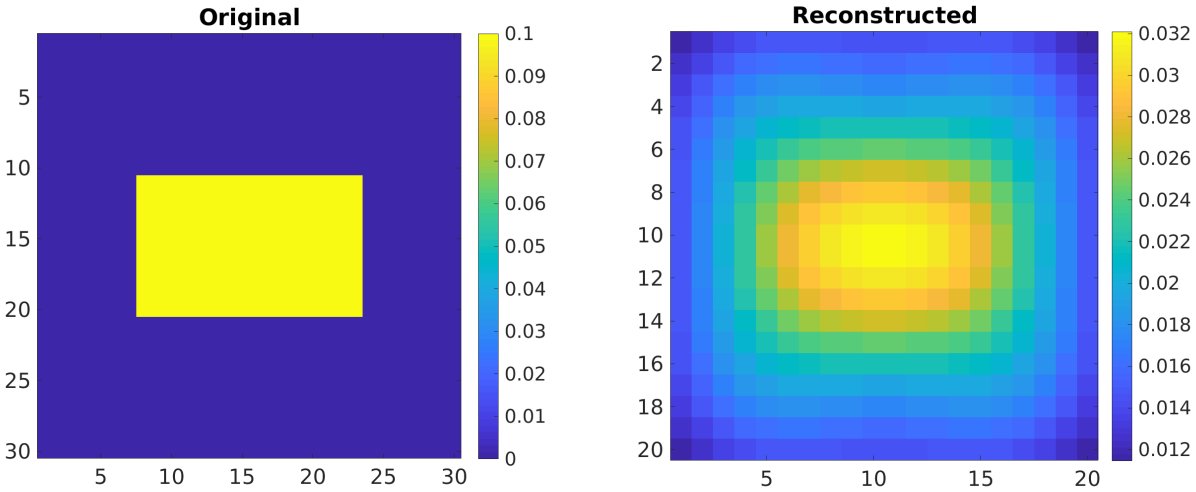

Figure 8: $\chi = 0.1$ and $frequency = 100Mhz$

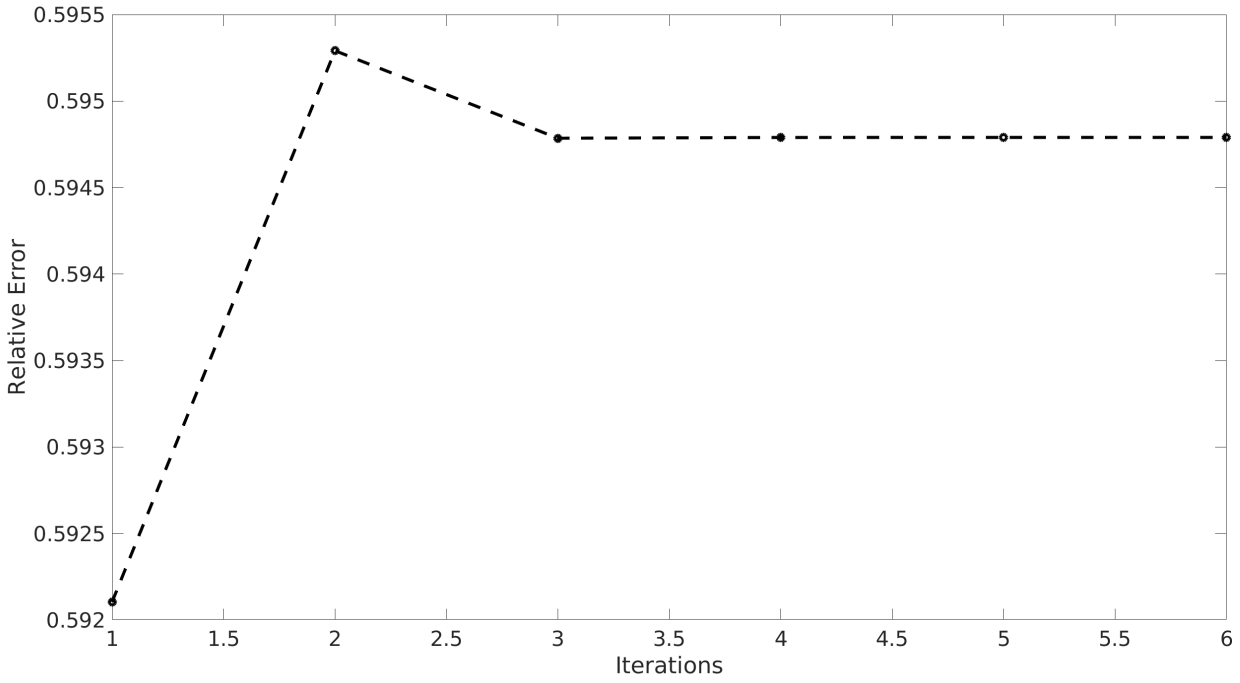

Figure 9: Variation of relative error for the figure 8

Figure 10 shows the variation of contrast error with gamma for its redefined value in 7. This result is limited to positive and moderately negative power of gamma. The highly negative power of gamma has been omitted i.e for $\gamma = 10^{-}12$, the contrast error was equal to $4.9 * 10^4$.

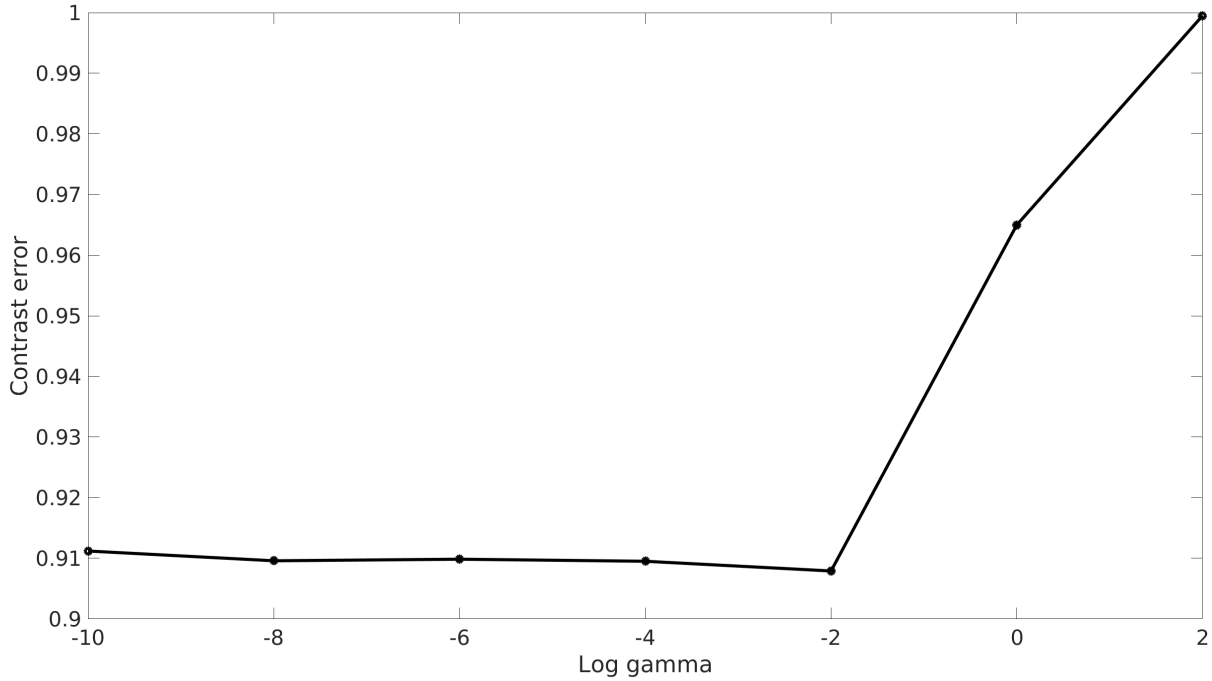

Figure 10: Variation of contrast error for figure 2 with redefined contrast error

4 Distorted Born Iterative Method(DBIM)

4.1 Definitions

This section describes the basic technique implemented in DBIM. The forward model followed is same as in 4. The idea behind DBIM is to update every quantity with respect to its previous value instead of the absolute value. In this regard, at each step, instead of minimising the absolute value of cost function, the problem is modified to minimize the difference between consecutive contrasts and current error between approximated and measured scattered field.

4.1.1 Updating Green's function

In order to accommodate the general Maxwell's equation with the difference in the fields instead of absolute fields, the Green's function need to be updated at each step. The equation for updating Green's function is as follows:-

$$G_1(r, r') = G(r, r') + \int_{\Omega} k_o^2 \chi(r") \, G_1(r", r') \, G(r, r") \, dr" \;\; r, r" \in \Omega, \;\; r' \in \Gamma \tag{8}$$

Accordingly, the data equation changes as

$$E^{scat}(r) = \int_{\Omega_{r'}} k_o^2 \chi(r') E^(tot)(r') G_1(r, r') \, dr' \;\; r \in \Omega, \;\; r' \in \Gamma \tag{9}$$

which, along with 4 and 8, gives the equation for updating contrast after two successive iterations,

$$E^{scat}_{meas}(r) - E^{scat}_{cal}(r) = \int_{\Omega_{r'}} k_o^2 (\chi_{i+1}(r') - \chi_i(r')) E^{tot}_i(r') G_1(r, r') \, dr' \;\; r \in \Omega, \;\; r' \in \Gamma \tag{10}$$

4.2 Algorithm

The concerned equations in DBIM can be casted into a compact form following the same procedure as in BIM. Consequently the following algorithm was implemented.

Algorithm 2 DBIM

$d_v \leftarrow e_v$

$$\chi \leftarrow [(G_s D_v)^\dagger (G_s D_v) + \gamma I]^{-1} (G_s D_v)^\dagger s$$

while $Convergence \neq True$ **do**
    Update d_v using 4
    Update Green's function(G_{new}) using 8
    Update s_{cal} using 9

$$\delta \leftarrow [(G_{new} D_v)^\dagger (G_{new} D_v) + \gamma I]^{-1} (G_{new} D_v)^\dagger (s - s_{cal})$$

    Update contrast as $\chi_{i+1} = \chi_i + \delta$
    Approximate s_v and check relative error(RE) using 6
    if $RE < threshold$ **then**
        $Convergence = True$
    else
        $Convergence = False$
return χ ▷ Reconstructed contrast

4.3 Results

The algorithm was tested on the following scatterers of size $\lambda/2 \times \lambda/3$ with a forward discretization of $\frac{\lambda}{20}$ and that of the reverse was as mentioned for a contrast of 0.5 and 1.

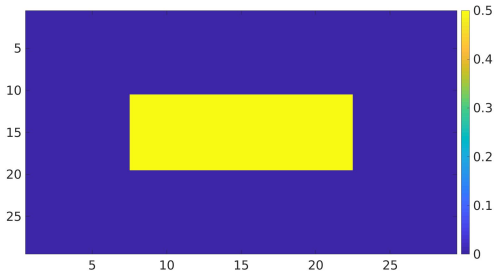

Figure 11: Original object

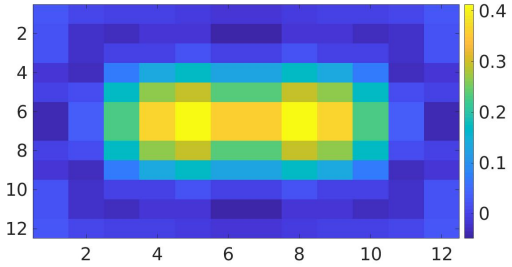

Figure 12: $\chi = 0.5$, $Discretization = \lambda/10$

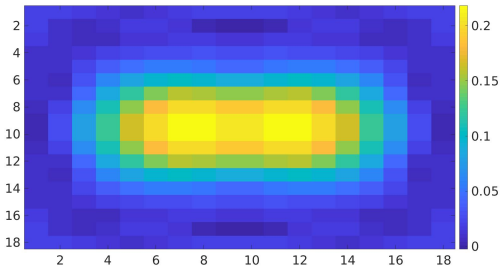

Figure 13: $\chi = 0.5$, $Discretization = \lambda/15$

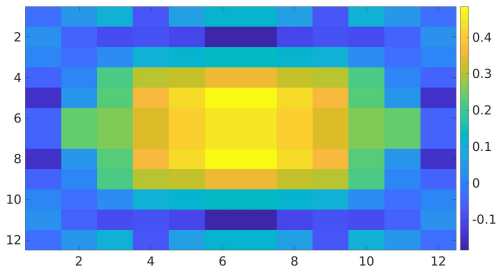

Figure 14: $\chi = 1$, *Discretization* $= \lambda/10$

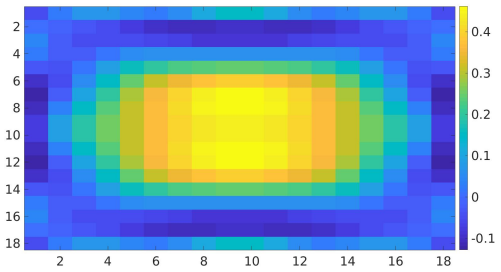

Figure 15: $\chi = 1$, *Discretization* $= \lambda/15$

Simulations were also run to test the dependence of reconstruction on regularization factor γ.

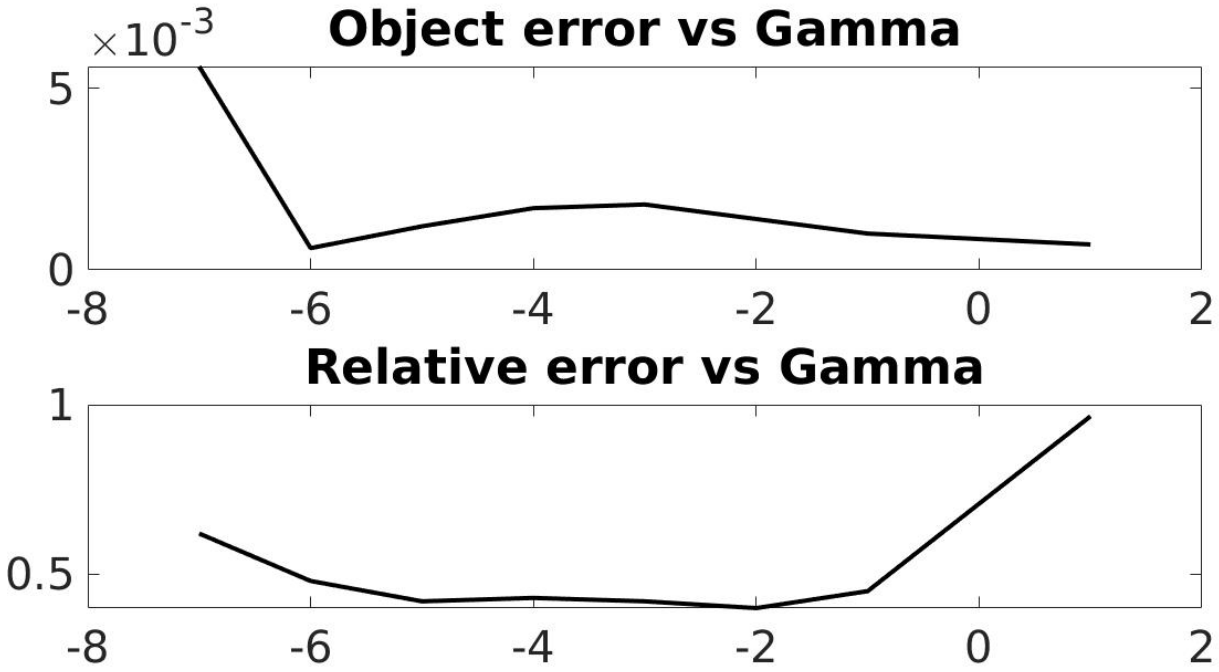

Figure 16: $\chi = 0.5$, *Discretization* $= \lambda/10$

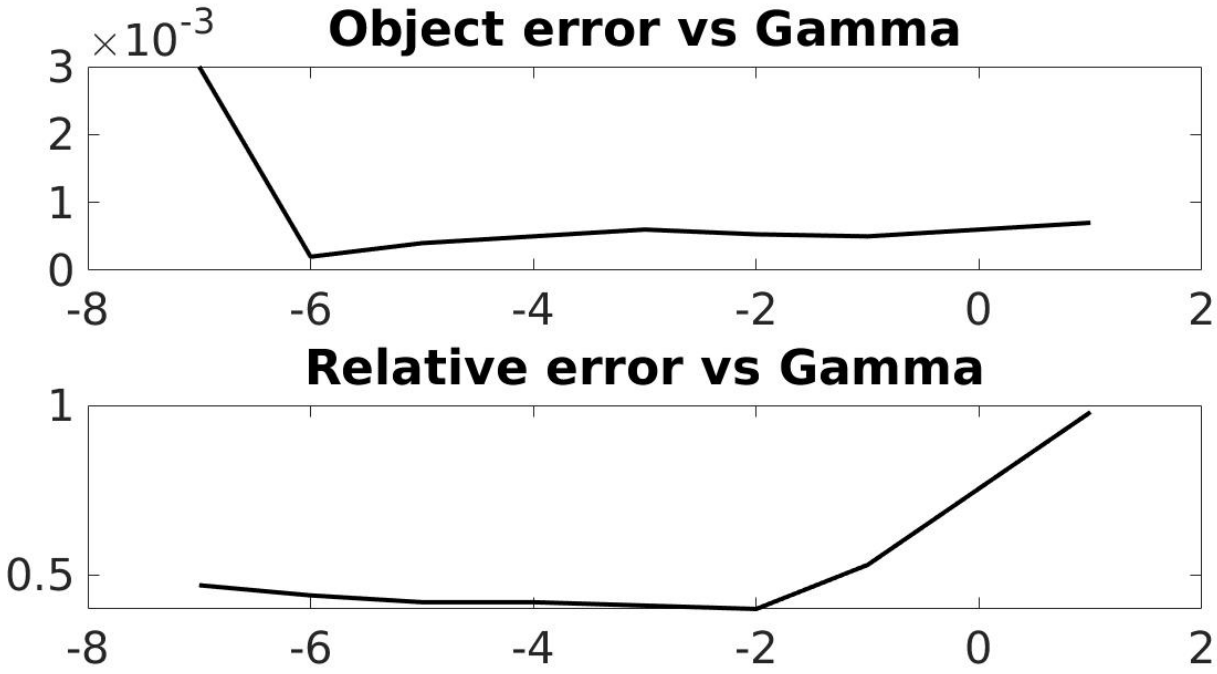

Figure 17: $\chi = 0.5$, $Discretization = \lambda/15$

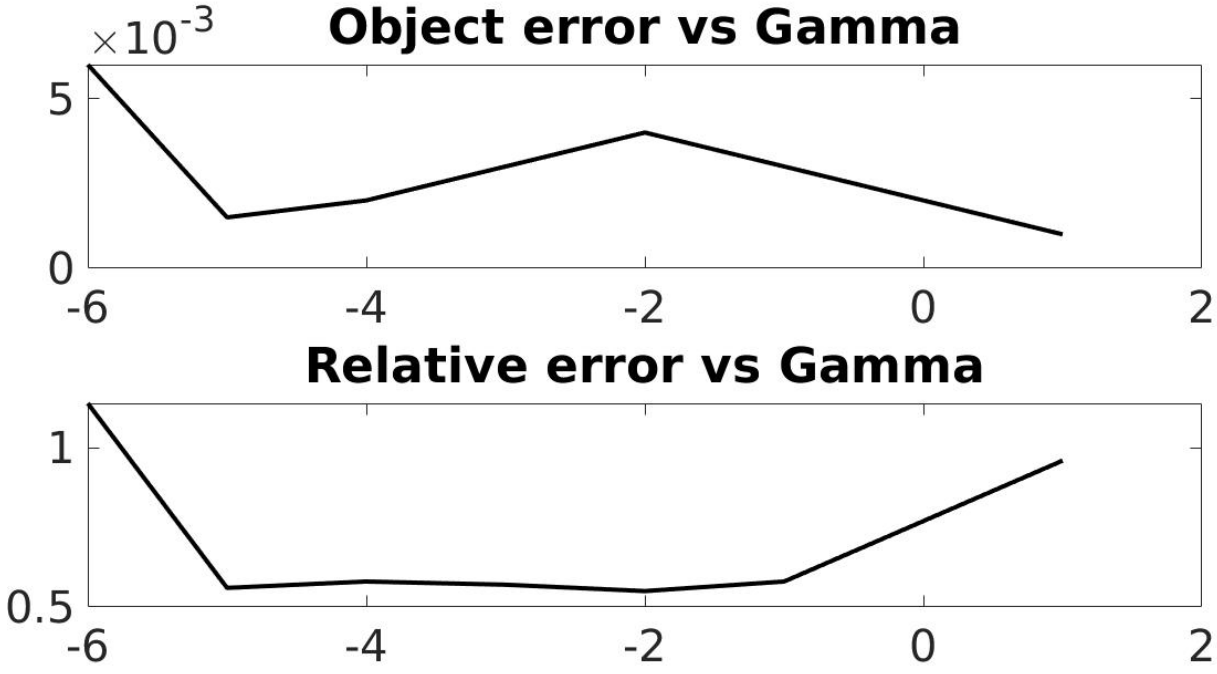

Figure 18: $\chi = 1$, $Discretization = \lambda/10$

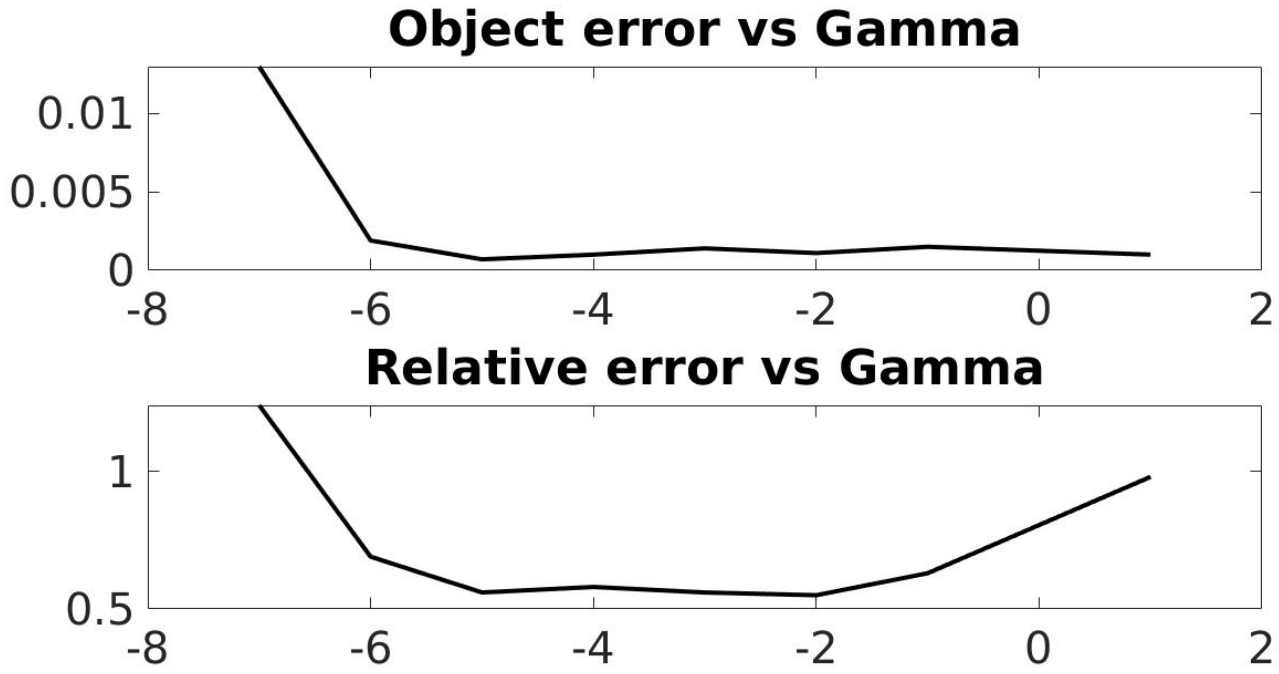

Figure 19: $\chi = 1$, $Discretization = \lambda/15$

5 Subspace Optimization

5.1 Definitions

This section analyses the matrix properties of G_s from 3, and w_v, where

$$w_v = x * d_v \tag{11}$$

and $*$ implies element wise multiplication. Thus G_s can also be written as

$$G_s w_v = s_v \tag{12}$$

An attempt was made to separate out the null space and the signal space (which is deterministic), in order to reduce both the computational cost and non-uniqueness of the inverse problem. The parameters and the error measures are defined as follows :-

$$\text{Effective Nullspace Component} = \frac{100}{Ni} \times \sum_{i=1}^{Ni} \frac{||w_v - w_{s_v}||}{||w_v||}\% \tag{13}$$

$$\text{Signal space Component} = \frac{100}{Ni} \times \sum_{i=1}^{Ni} \frac{||w_{s_v}||}{||w_v||}\% \tag{14}$$

$$\text{Error in } s = \frac{100}{Ni} \times \sum_{i=1}^{Ni} \frac{|{s_v}^{\text{true}} - {s_v}^{\text{approx}}||}{||{s_v}^{\text{true}}||}\% \tag{15}$$

where, signal space of w_v is $w_{s_v} = w_v - w_{n_v}$, Ni is the number of transmitters, ${s_v}^{\text{true}}$ is the measured scattered field and ${s_v}^{\text{approx}}$ is the calculated scattered field from the reconstructed profile.

Following 12 and the SVD of G_s, $G_s = U \sum V$,
we can define the signal space of contrast source w_v as,

$$w_{s_v} = \sum_{j=1}^{L} \frac{u_j^H s_v}{\sigma_j} v_j \tag{16}$$

using the first L singular values of G_s. Besides, using definition of SVD, we can write

$$w_{s_v} = \sum_{j=1}^{L} v_j^H w_v v_j \tag{17}$$

where v_j and u_j are j^{th} columns of U and V and σ_j is the j^{th} diagonal element of $\sum$.

5.2 Results

Figure 11 - 17 show results for the noiseless data and 18 - 21 show those for the noisy data.

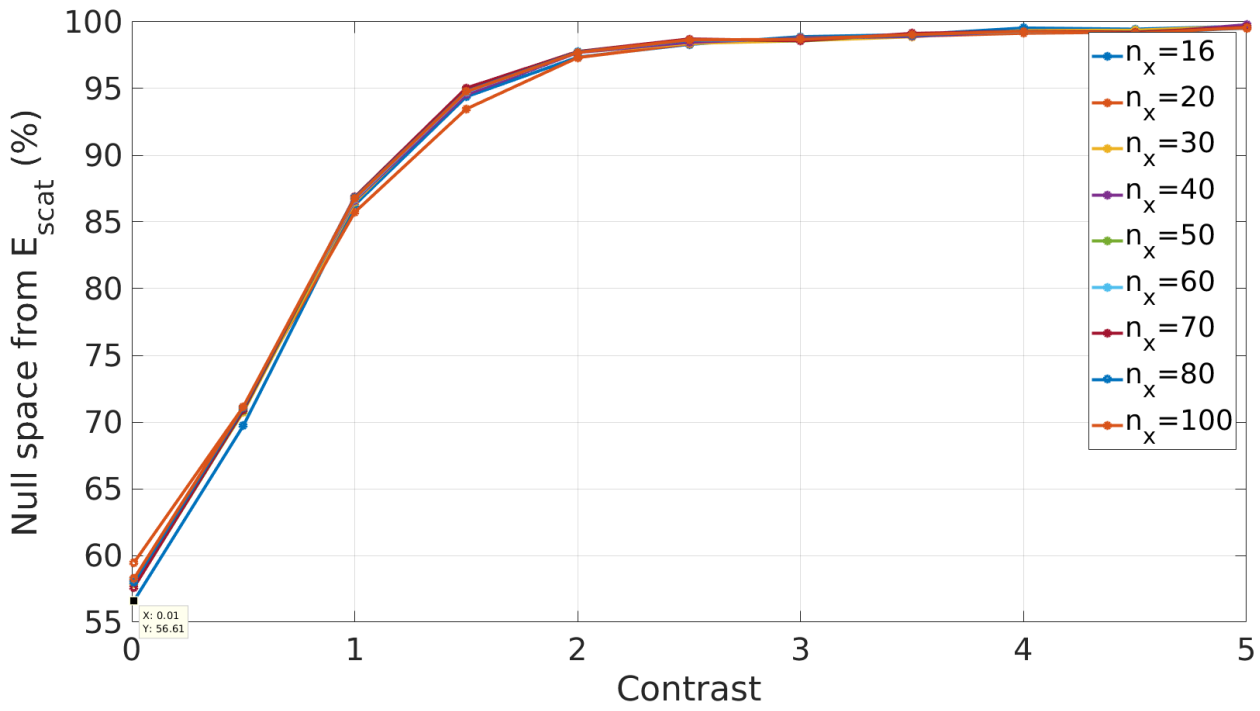

Figure 20: Effective Nullspace component from 's' as a function of increasing contrast is shown, at different discretization levels. It is observed that Effective Nullspace components increases with increase in contrast and discretization (But not very much sensitive for sufficiently large(= 16) discretization. Top 32 singular components of G_s.

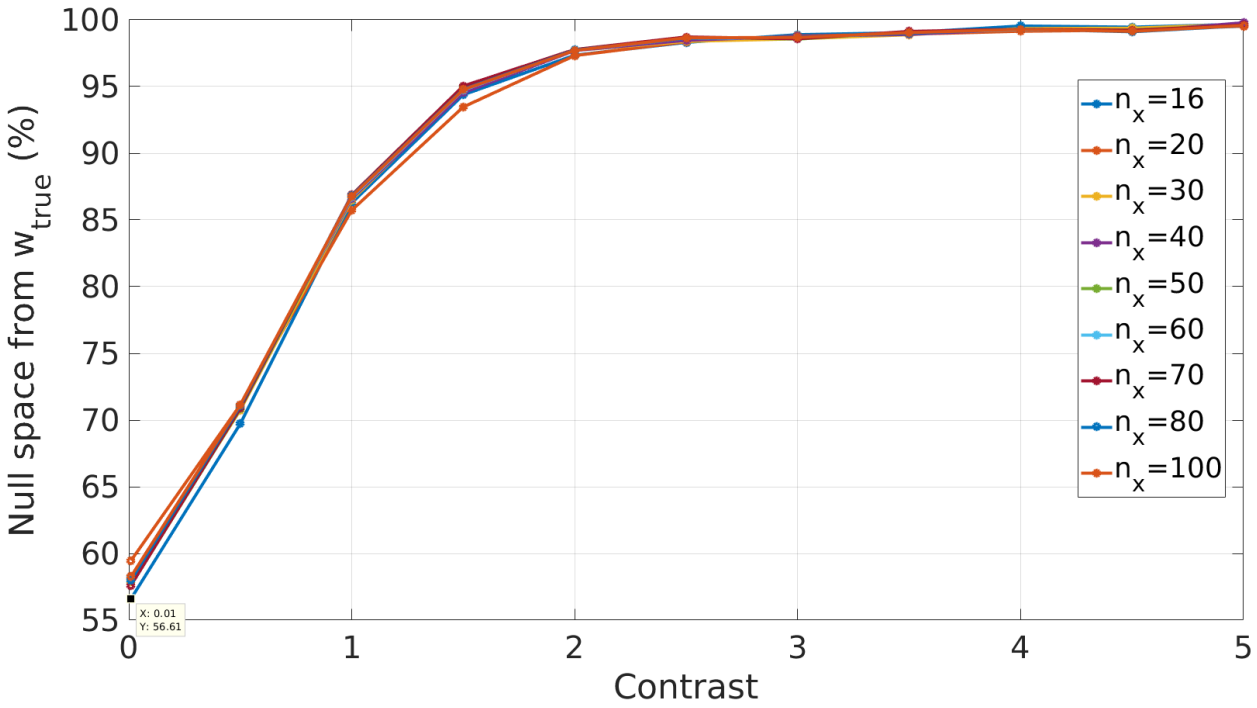

Figure 21: Effective Nullspace component from true 'w_i' as a function of increasing contrast is shown, at different discretization levels. It is observed that Effective Nullspace components increases with increase in contrast and discretization (But not very much sensitive for sufficiently large(= 16) discretization. Effective Nullspace components from true 'w_i' and 's' are same. Top 32 singular components of G_s.

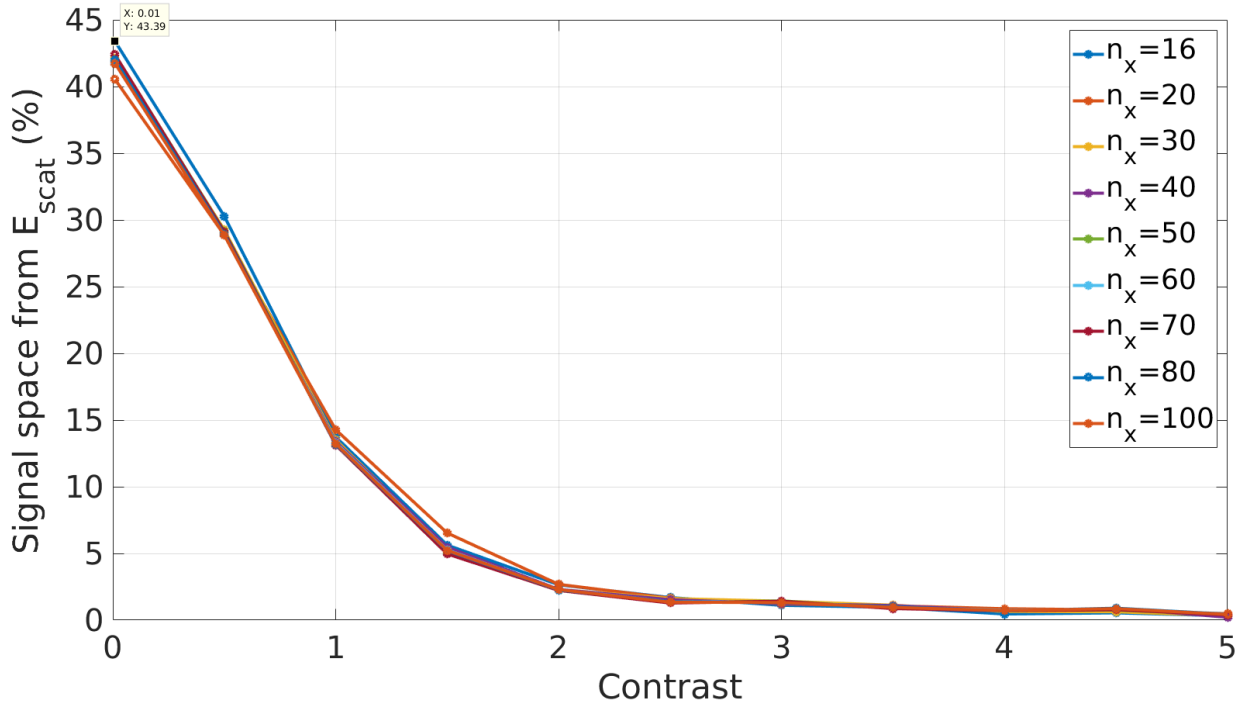

Figure 22: Signalspace component from 's' as a function of increasing contrast is shown, at different discretization levels. It is observed that signalspace components decreases with increase in contrast and discretization.Top 32 singular components of G_s.

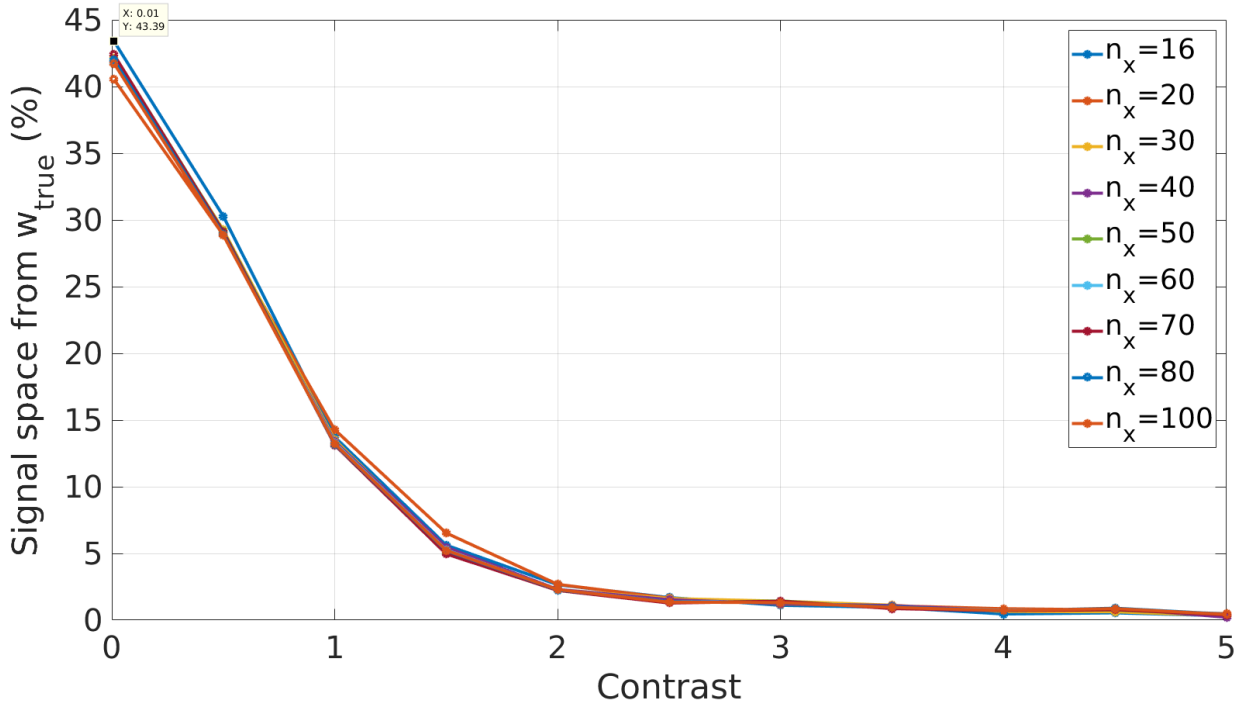

Figure 23: Signalspace component from true 'w_i' as a function of increasing contrast is shown, at different discretization levels. It is observed that signalspace components decreases with increase in contrast and discretization. Top 32 singular components of G_s.

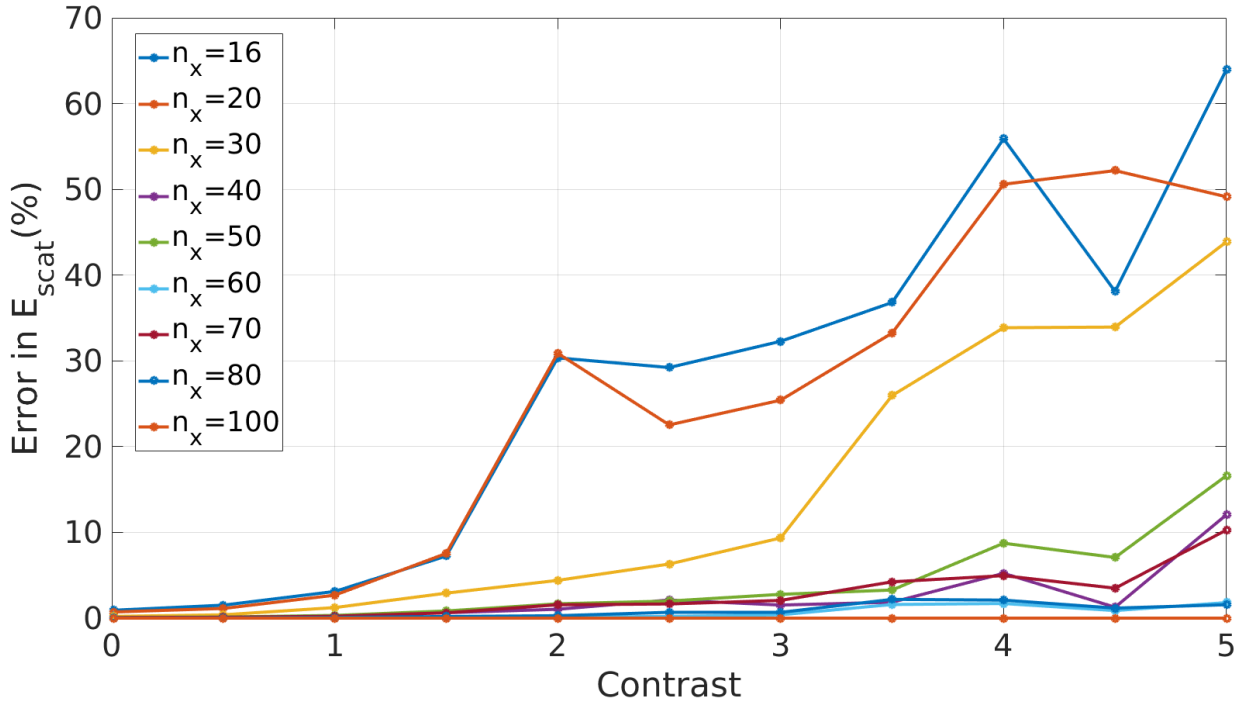

Figure 24: Error in s at n_x discretization with respect to s at very high discretization. It is high for lower discretizations.

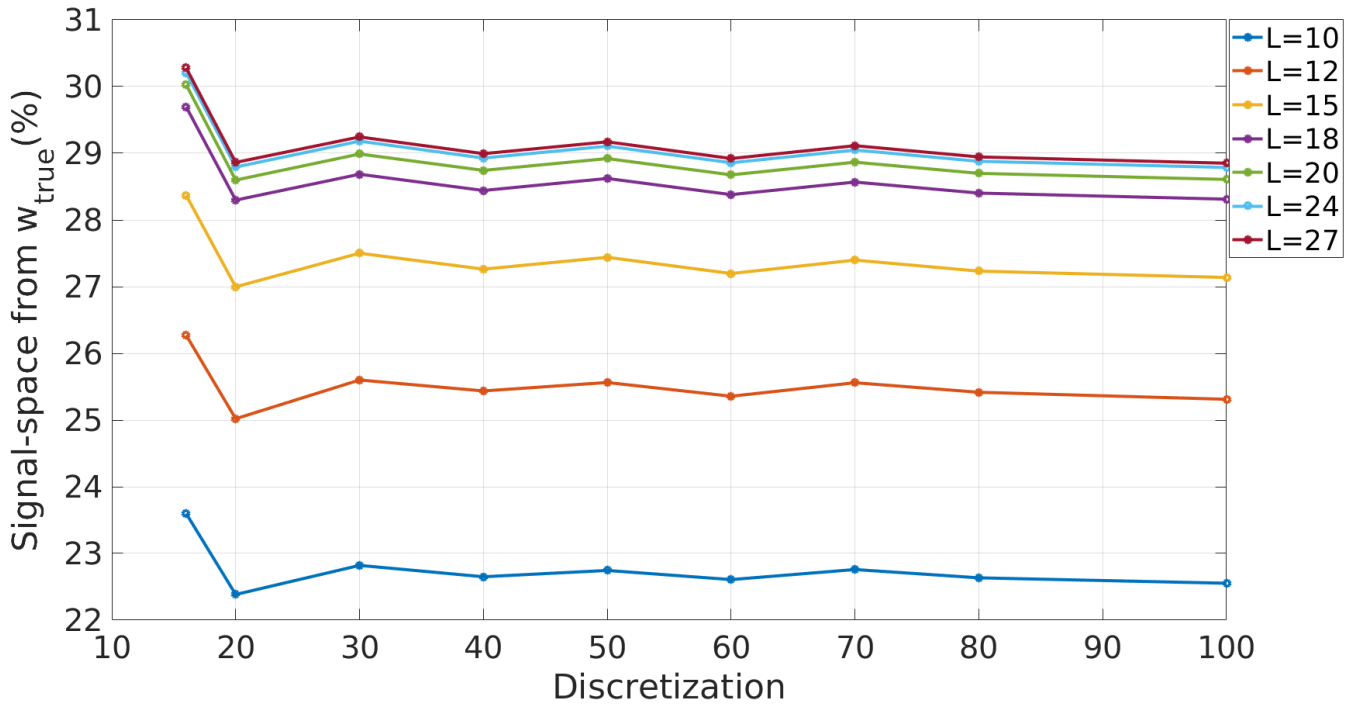

Figure 25: Variation of row space of true 'w_i' with discretization for different values of L at $\chi = 0.5$. It can be observed that the row space is not sensitive to the value of L after a certain value (18).

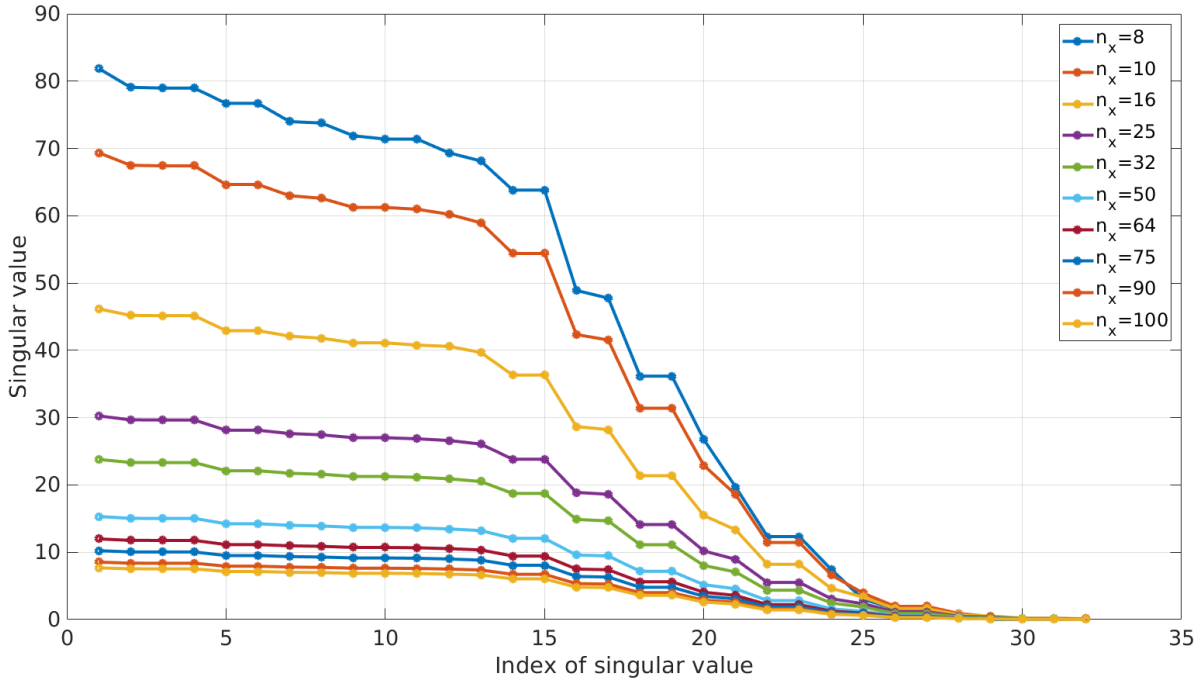

Figure 26: Fall of singular values with discretization. For a value of L between 15 and 20, the decay of singular values is fast.

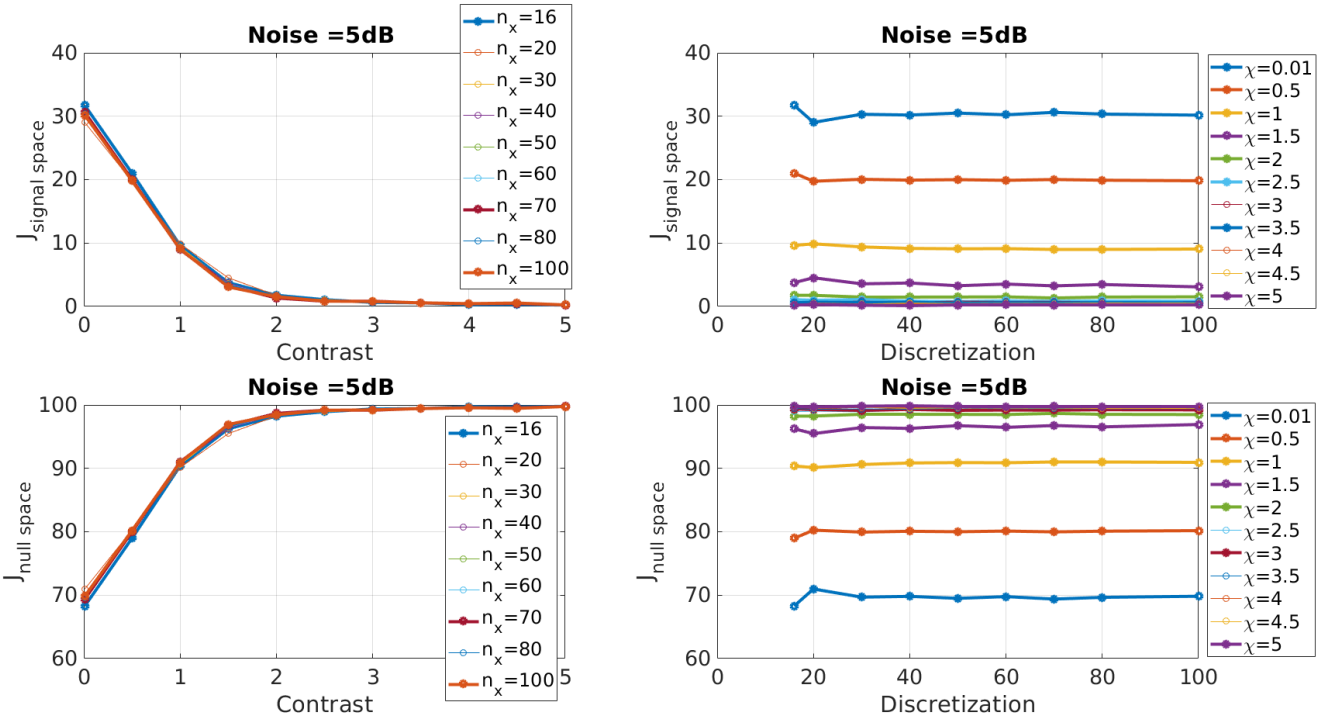

Figure 27: Variation of signal space and null space components with discretization and contrast for a noise of 5dB.

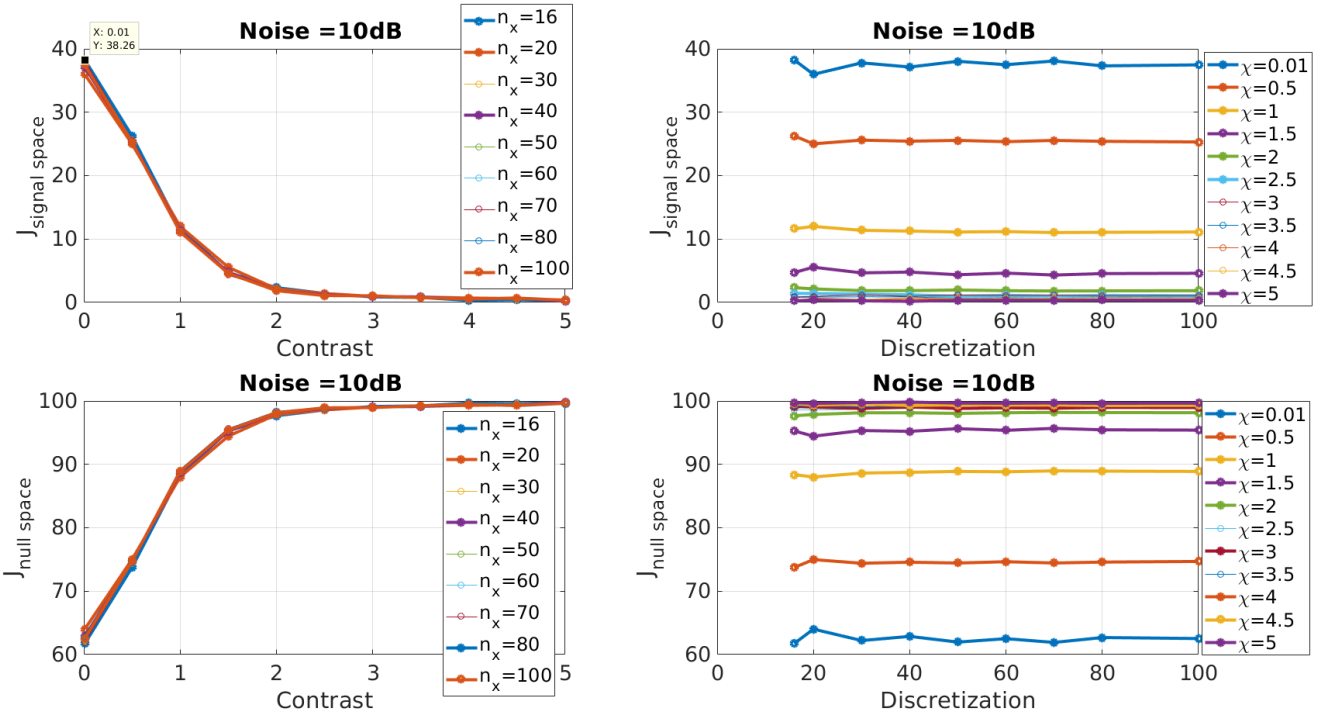

Figure 28: Variation of signal space and null space components with discretization and contrast for a noise of 10dB.

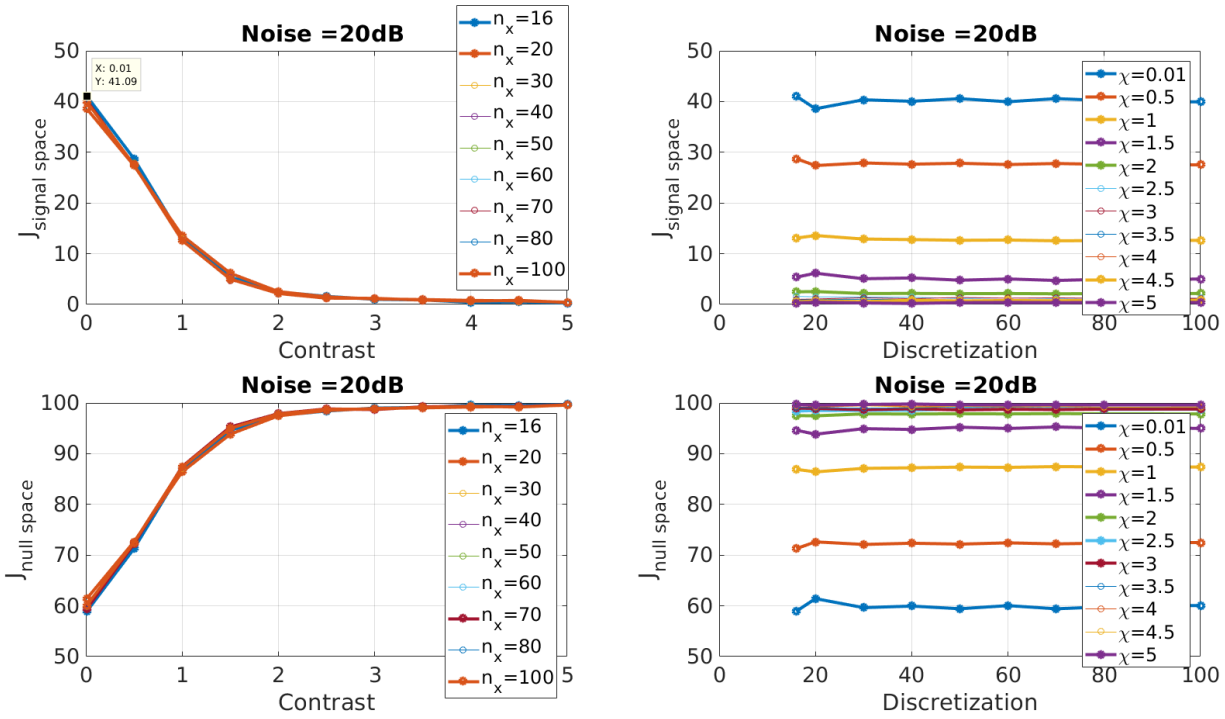

Figure 29: Variation of signal space and null space components with discretization and contrast for a noise of 20dB.

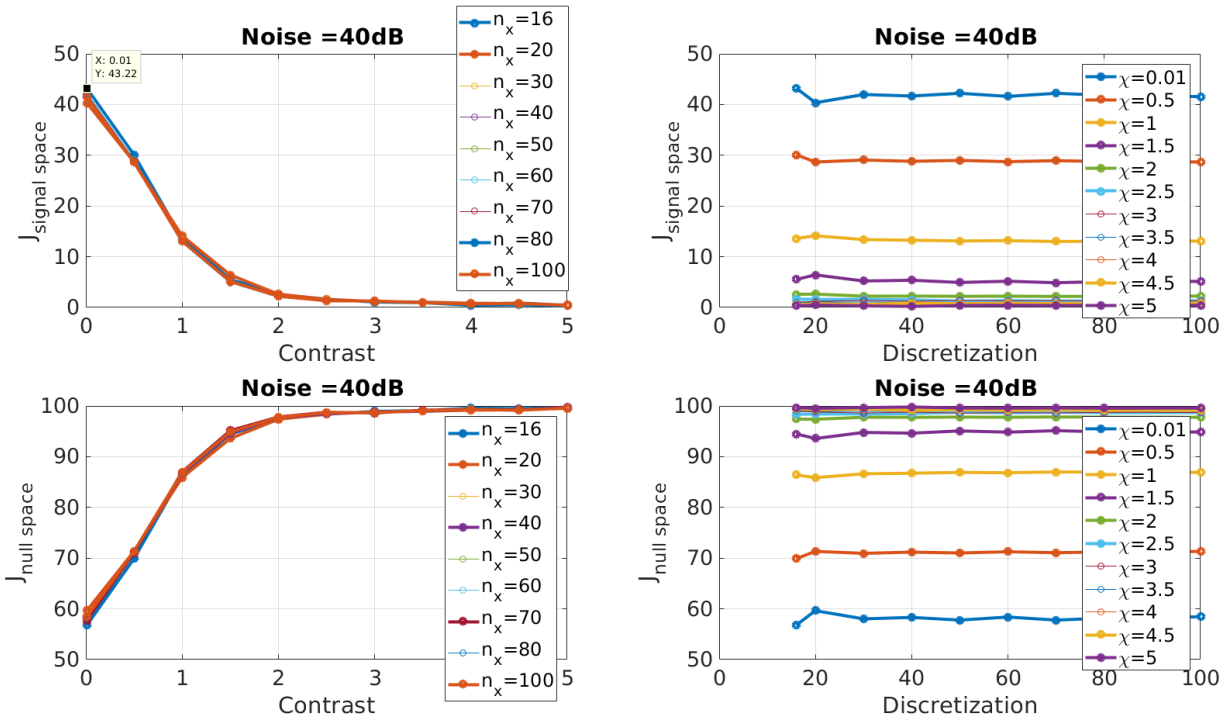

Figure 30: Variation of signal space and null space components with discretization and contrast for a noise of 40dB.

5.3 Conclusion

It is established that the signal space information stored in the contrast source w decreases exponentially with the contrast and stays almost constant with discretization. Moreover, the number of singular values used for determining the signal space, as can be seen from figure 17, need not be higher than a certain number for a specified contrast, as the values tend to diminish sharply.

6 Edge detection

6.1 DUC

This section will give a concise introduction to the previous attempt on adaptive mesh transformation. For more details, the reader is directed to [6]. DUC is an iterative procedure of dividing and uniting coarse pixels based on the information given by the gradient at fine pixels. The important aspects are as follows :-

1. **T-matrix**: The clustering of pixels is guided by the transformation of the T-matrix at each iteration. T-matrix acts on the contrast vector x to define the clustering of pixels into super-pixels $\tilde{x}$ at every iteration. The evolution of the T-matrix is further guided by the gradient of the cost function and the heuristically determined thresholds.

2. **Division**: The breakdown of each super-pixel in the coarse mesh, $\widetilde{\mathbf{x}}$, is determined by the gradient of cost function, J at each $x_i \in \mathbf{x}^*$, such that

$$\nabla_{\mathbf{x}^*} \mathrm{J} = (G_s D_v)^\dagger (G_s D_v \mathbf{x}^* - s_v) \tag{18}$$

   where $\mathrm{A}^\dagger$ and A^* imply conjugate transpose and conjugate of A, respectively.
   Now, each $x_i^{(n)}$, where n is the index of the super-pixel k_n to which it belongs, is considered for separation from its super-pixel based on predetermined thresholds.

3. **Unification**: After reconstruction, the effective domain under investigation is further reduced by merging super-pixels in the coarse mesh according to their reconstructed values using Algebraic Reconstruction Technique [8]. A pair of super-pixel is considered for unification if the difference between the reconstructed values is less than a pre-defined threshold.

6.2 Detecting edges

A picture of the gradient of the cost function with respect to fine pixels have been observed to have edges at disapproving values of contrast as can be seen in figure 24.

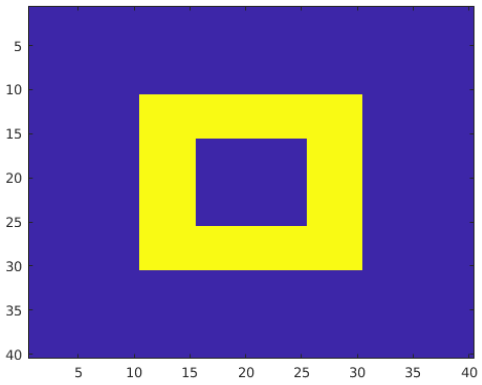

Figure 31: Original Object

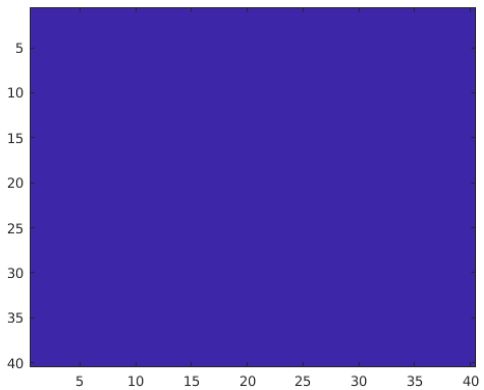

Figure 32: Initialization contrast= 0

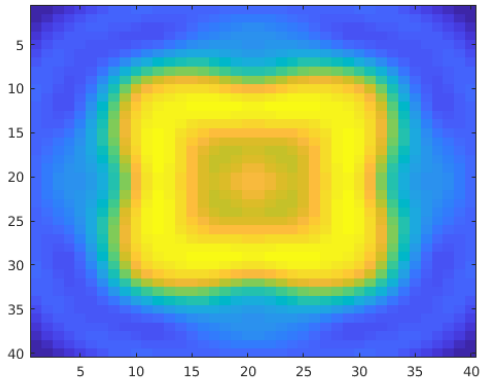

Figure 33: Gradient at the initialization step for all contrast= 0

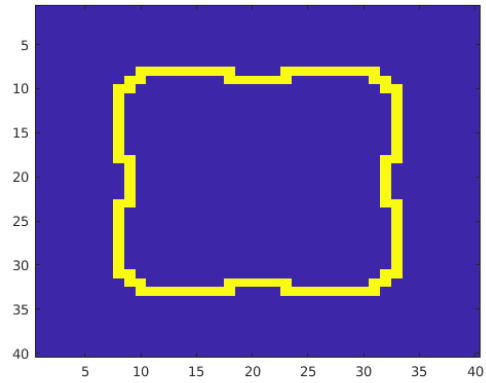

Figure 34: Edge detected in the gradient using Canny edge detection technique

Based on the above observation, that the true value of contrast at fine pixels would enforce a low and uniform gradient (as in figure 26), the gradient can be exploited to iteratively zoom inside the convex hull detected at each step. This procedure attempts to reconstruct the support of the scatterer assuming the contrast value is known. As of now, the number of contrasts are limited to 2; as the work proceeds, the algorithm can be extended to recover the support for multiple contrasts.

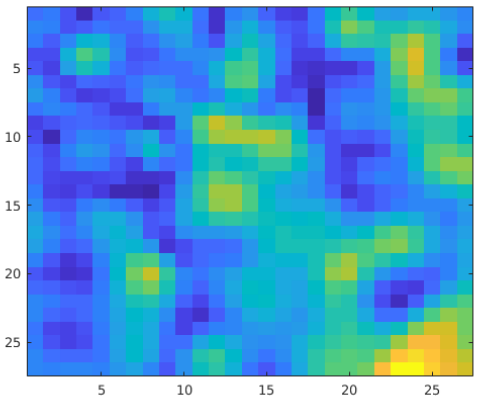

Figure 35: Gradient of cost function for true contrast

6.3 Variation of performance with different edge detection techniques

The performance of the algorithm depends heavily on the performance of the edge detecting algorithm. To ensure accuracy about and uniformity in the edge detecting criterion across iteration, 3 broad criteria were tried out for the first two consecutive iterations.

1. Canny:

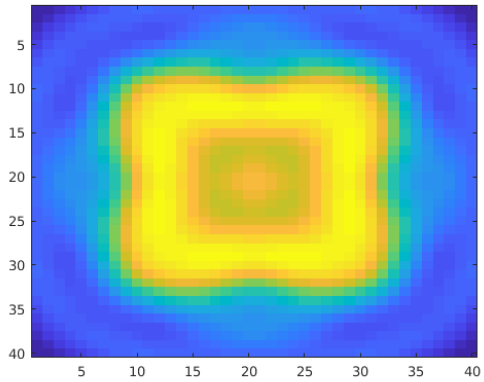

Figure 36: Gradient at step 1

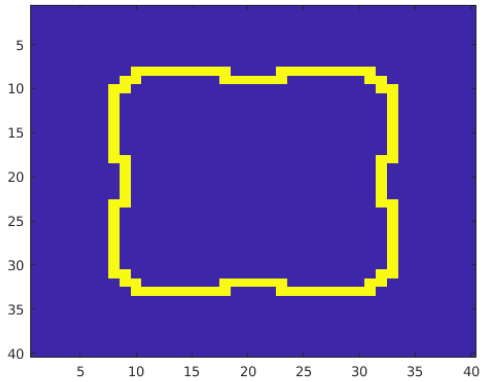

Figure 37: Edge detected by Canny's algorithm at step 1

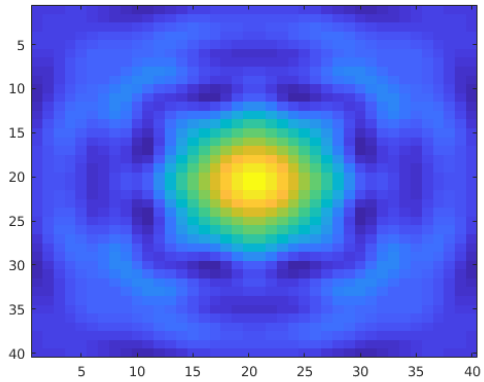

Figure 38: Gradient at step 2 using Canny detected boundary

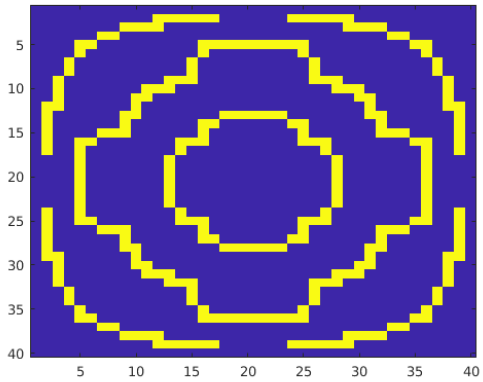

Figure 39: Edge detected by Canny's algorithm at step 1

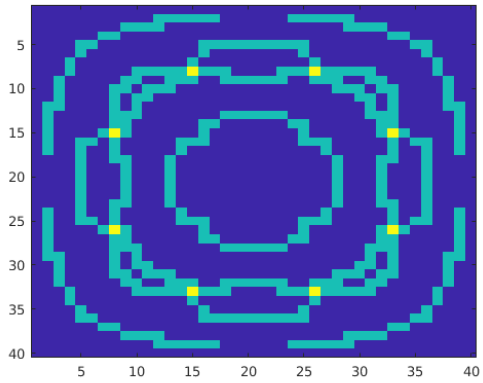

Figure 40: Union of the edges detected in consecutive iterations by Canny

2. Laplacian of Gaussian:

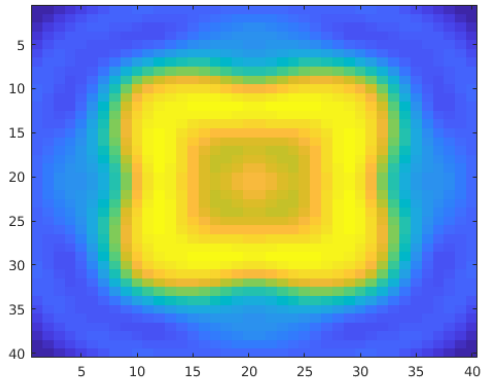

Figure 41: Gradient at step 1

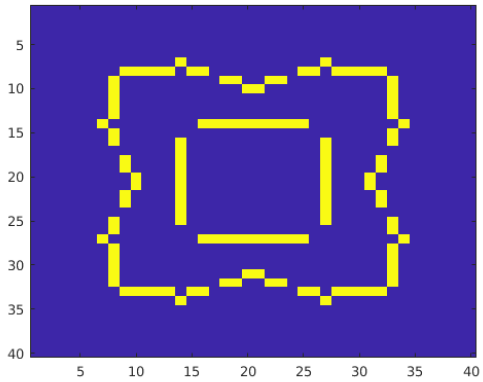

Figure 42: Edge detected by considering the zero crossings of the Laplacian of Gradient(LoG) picture at step 1

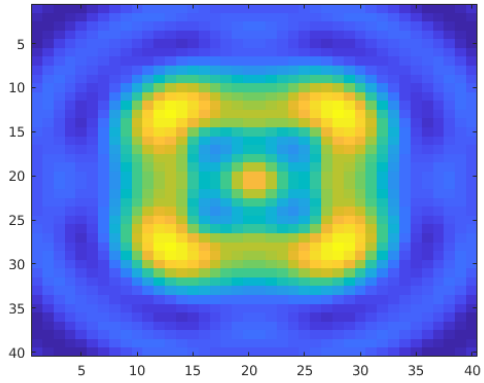

Figure 43: Gradient at step 2 using LoG detected boundary

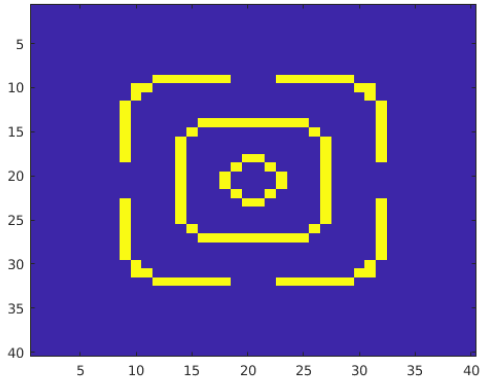

Figure 44: Edge detected by considering the zero crossings of the laplacian of the gradient picture at step 2

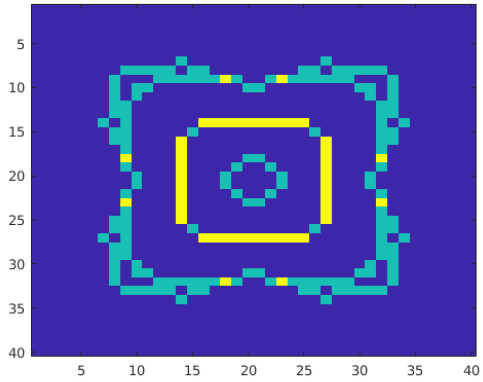

Figure 45: Union of the edges detected in consecutive iterations by LoG

3. First order (Sobel):

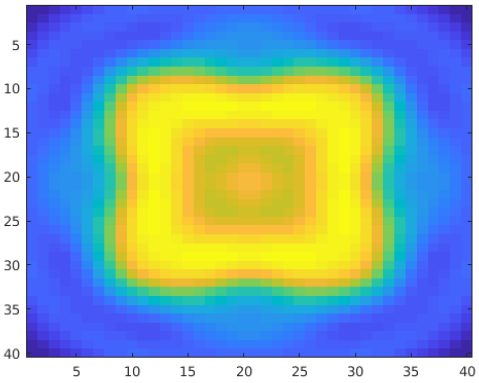

Figure 46: Gradient at step 1

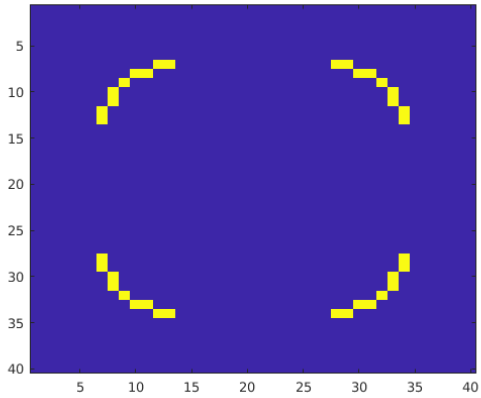

Figure 47: Edge detected by first order derivatives of the gradient picture at step 1

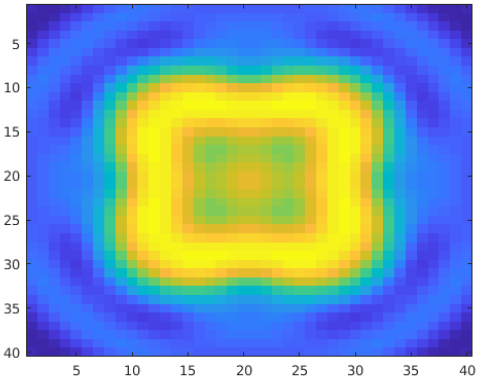

Figure 48: Gradient at step 2 using Sobel detected boundary

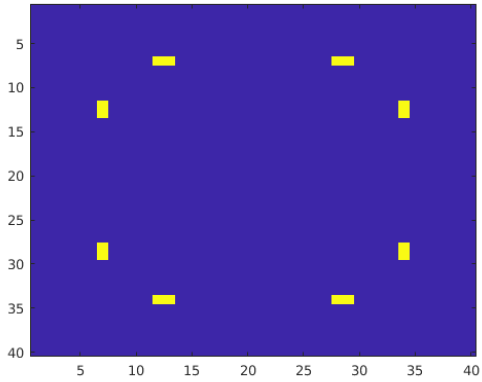

Figure 49: Edge detected by first order derivatives of the gradient picture at step 2

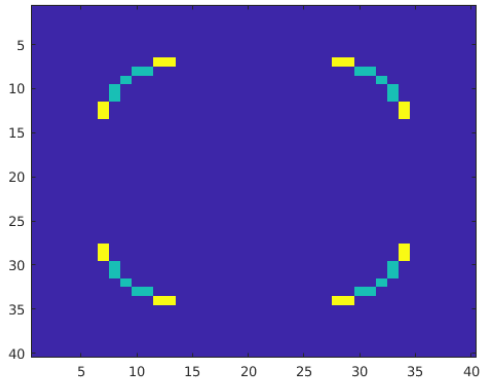

Figure 50: Union of the edges detected in consecutive iterations by Sobel

6.4 Conclusion and Future work

Results of LoG is seen to be the best approximate of the scatterer as of yet. Further, the edge linking technique given here was tried out without success. The reason for this was guessed as the absence of conventional edges.

Further, better edge detecting techniques present in the literature (as reviewed so far), such as [9] and [10] which can be implemented so as to eliminate the need of edge linking altogether.

7 Level set method

7.1 Introduction

Level-set based methods have previously been used in microwave imaging for multimaterial recovery, as in [5]. But the algorithm presented assumes a discrete variation of contrasts which is not very pragmatic. The current report is an attempt at modelling the continuous variation of contrasts and extending the aforementioned algorithms for the recovery of the same. We assume the value of contrast is known. The idea is to represent the variation of contrasts using a sigmoid function instead of a unit step function.

7.2 Extension of the level set formulation to continuous distribution of contrast

The idea is to use a logistic sigmoid function,

$$s(t) = \frac{a}{1 + e^{-kt}} \tag{19}$$

to approximate the Heaviside function,

$$u(t) = \begin{cases} 1 & \text{if } t < 0 \\ 0 & \text{if } t \geq 1 \end{cases} \tag{20}$$

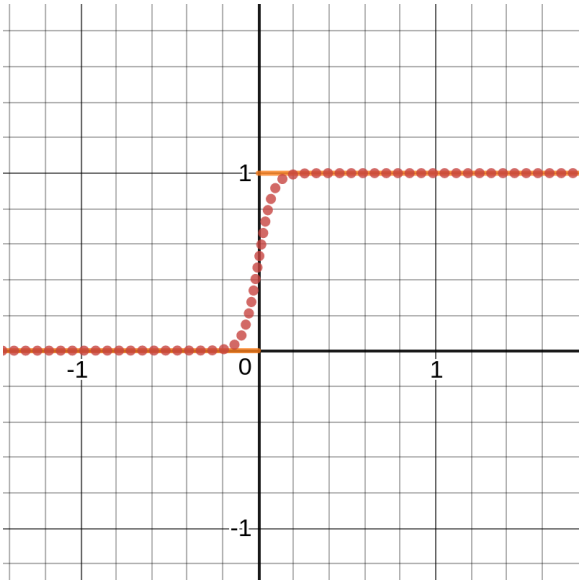

Figure 51: Approximating the Heaviside function with the logistic sigmoid with $a = 1$ and $k = 25$

As mentioned in [11] and [12], the heaviside function can be approximated with the logistic sigmoid function with a controllable error, d as a function of k in $s(t)$. Drawing as in [12] and with notations defined in [5], validation of the function as suitable for material recovery has been worked out.

7.3 The one with two contrasts

According to the current idea, the contrast can be represented as,

$$\chi(r') = \chi_i s(\phi(r')) + \chi_e(1 - s(\phi(r'))) \tag{21}$$

The cost function is defined as

$$J = \|s_v - G_S D_v x\|_2^2 \tag{22}$$

This cost function is minimized as the level-set function evolves over time as

$$L(\phi) = \frac{\partial \phi}{\partial t} = -\frac{\partial J}{\partial \phi} \tag{23}$$

The right hand side above can be expressed as

$$\frac{\partial J}{\partial \phi} = \frac{\partial J}{\partial \chi}\frac{\partial \chi}{\partial \phi} \tag{24}$$

From 22, we have

$$\frac{\partial J}{\partial \chi} = |(G_S D_v)^\dagger (G_S D_v \chi - s_v)| \tag{25}$$

From 21, we have

$$\frac{\partial \chi}{\partial \phi} = (\chi_i - \chi_e)\frac{k}{(1+e^{(-k\phi)})^2} \tag{26}$$

Thus from 25 and 26, we see that the convergence rate of the cost function, defined as

$$\frac{\partial J}{\partial t} = -(\frac{\partial J}{\partial \phi})^2 \tag{27}$$

depending on the value of k, might actually be higher than that in case of Heaviside function.

7.4 The one with multiple contrasts

For multiple contrasts, a sum of scaled and shifted sigmoid functions can be defined

$$s(l, x; \phi) = \sum_{i=1}^{N} x_i s(\phi - l_i) \tag{28}$$

So the contrasts can be expressed for multiple level-set functions, with each sigmoid giving a high response on multiple intervals, as done in [5]

$$\chi(r') = \sum_{i=1}^{N} \chi_i \prod_{j=1}^{N_1} s(\phi_j \geq l_{ij} \quad \& \quad \phi_j < l_{ij+1}) \tag{29}$$

where N is the number of intervals a sigmoid needs to be active for and N_1 is the number of level set functions. Working out for a 3 material case, we have $N_1 = 2$ and $N_{(1)} = N_{(2)} = 2$,

$$\begin{aligned}\chi(r') = \chi_1 s(\phi_1 > -\infty \quad \& \quad \phi_1 < 0) s(\phi_2 > -\infty \quad \& \quad \phi_2 < 0) \\ + \chi_2 s(\phi_1 > -\infty \quad \& \quad \phi_1 < 0) s(\phi_2 > 0 \quad \& \quad \phi_2 < \infty) \\ + \chi_3 s(\phi_1 > 0 \quad \& \quad \phi_1 < \infty) s(\phi_2 > -\infty \quad \& \quad \phi_2 < 0) \\ + \chi_4 s(\phi_1 > 0 \quad \& \quad \phi_1 < \infty) s(\phi_2 > 0 \quad \& \quad \phi_2 < \infty)\end{aligned} \tag{30}$$

$$\begin{aligned}\chi(r') = \chi_1 (1 - \frac{1}{1+e^{-k\phi_1}})(1 - \frac{1}{1+e^{-k\phi_2}}) \\ + \chi_2 (1 - \frac{1}{1+e^{-k\phi_1}})(\frac{1}{1+e^{-k\phi_2}}) \\ + \chi_3 (\frac{1}{1+e^{-k\phi_1}})(1 - \frac{1}{1+e^{-k\phi_2}}) \\ + \chi_4 (\frac{1}{1+e^{-k\phi_1}})(\frac{1}{1+e^{-k\phi_2}})\end{aligned} \tag{31}$$

χ_3 and χ_4 can be put as equals.

That gives

$$\frac{\partial \chi}{\partial \phi_1} = \frac{k}{(1+e^{-k\phi_1})^2}\{(\chi_3 - \chi_1)s(-\phi_2) + (\chi_4 - \chi_2)s(\phi_2)\} \tag{32}$$

and

$$\frac{\partial \chi}{\partial \phi_2} = \frac{k}{(1+e^{-k\phi_2})^2}\{(\chi_2 - \chi_1)s(-\phi_1) + (\chi_4 - \chi_3)s(\phi_1)\} \tag{33}$$

Thus ensuring convergence of the method.

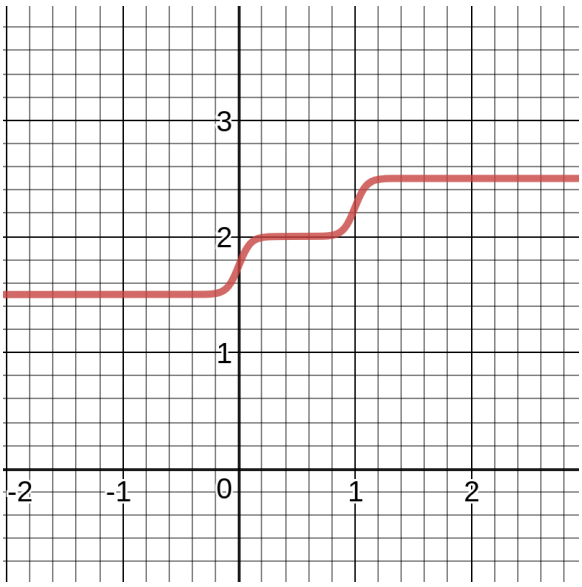

Figure 52: 3 different contrasts modeled with the Sigmoid function. The transition, to be noted, is smooth, unlike that in the case of Heaviside. Here, $\chi_1 = 0.5, \quad \chi_2 = 1, \quad \chi_3 = 1.5, \quad k = 20 \quad \& \quad l = 1$

7.5 Algorithm

This section explains the algorithm. The definitions used in the algorithm have been borrowed from [1] and [5].

Algorithm 3 Born Iterative Method using level-set evolution

procedure BIM(s_v, χ)
  $d_v \leftarrow e_v$
  while $Convergence_{outer} \neq True$ **do**
    Update χ using level-set solver
    $Costfunction_{old} = Costfunction$
    Initialize level-set function ϕ
    while $Convergence_{inner} \neq True$ **do**
      Solve the level-set equation: $\frac{\partial \phi}{\partial t} = -\frac{\partial J}{\partial \phi}$ ▷ Refer to 24
      Update level-set function: $\phi_{new} = \phi_{old} + \frac{\partial \phi}{\partial t}$
      Update values of contrast: $\chi = f(\phi_{new})$
      Update cost function.
      if $Costfunction - Costfunction_{old} < tolerance$ **then**
        $Convergence_{inner} = True$
      else
        $Convergence_{inner} = False$
    Update d_v ▷ Forward Problem
    Update $Costfunction$
    if $Costfunction < threshold$ **then**
      $Convergence_{outer} = True$
    else
      $Convergence_{outer} = False$
  return χ_{recon} ▷ Reconstructed contrast

7.6 Results

7.6.1 With $\phi_{initial}$ as a radial function of the grid

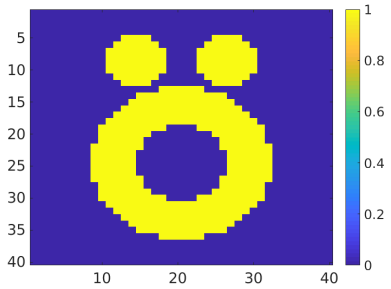

Figure 53: Original Scatterer

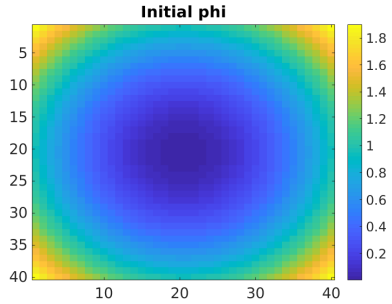

Figure 54: Initial level set function

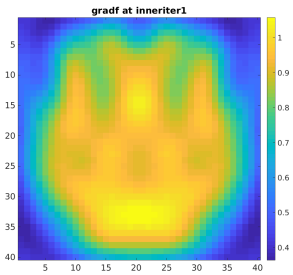

Figure 55: Gradient at first iteration of level set

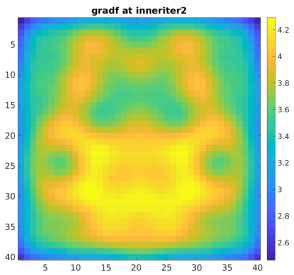

Figure 56: Gradient at second iteration of level set

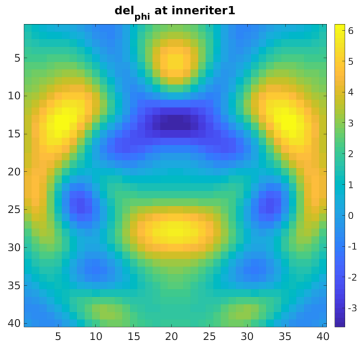

Figure 57: Evolution of phi at first level set iteration

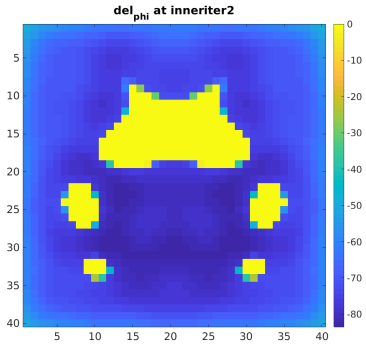

Figure 58: Evolution of phi at second level set iteration

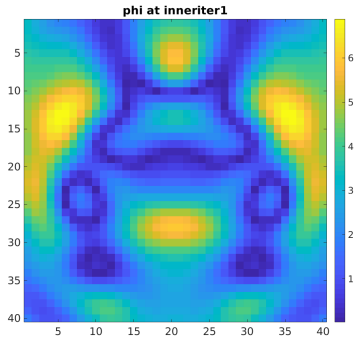

Figure 59: Phi at first level set iteration

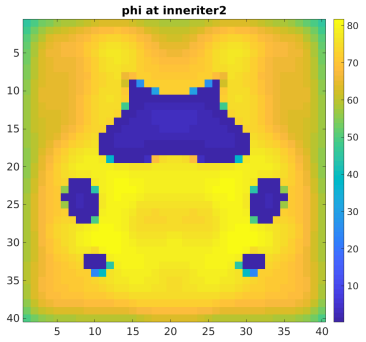

Figure 60: Phi at second level set iteration

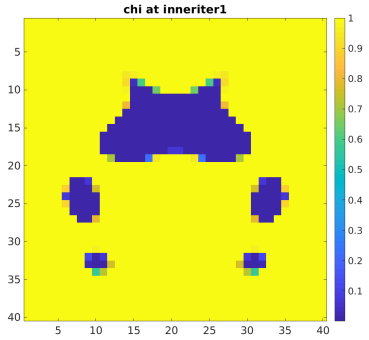

Figure 61: Chi at first level set iteration with $cf = 699175.16$

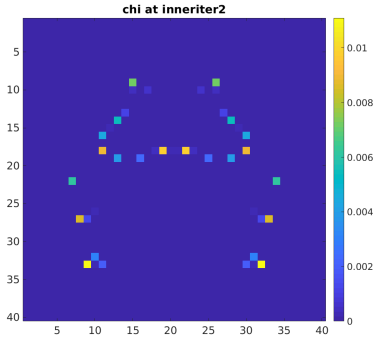

Figure 62: Chi at second level set iteration with $cf = 282.36$

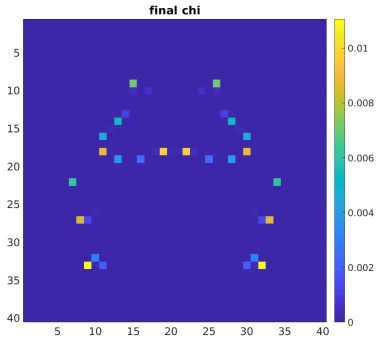

Figure 63: Final reconstruction with $cf = 282.36$

The reconstructions were also tried out with $\phi_{initial}$ as a zero on the grid. Results were hardly any better than the previous case and hence are not presented here.
A new level-set algorithm was implemented following the idea presented in [13]. The algorithm is followed by a concise description of the method.

1. An initial domain D is defined (as shown in 64) on which the contrast, χ is defined as

$$\chi(x) = \begin{cases} \chi_{int} & \text{if } x \in D \\ \chi_{ext} & \text{if } x \notin D \end{cases}$$

   D is related to level set function ϕ as $D = \{x|\phi(x) < 0\}$, so that χ is related to ϕ as

$$\chi(x) = \begin{cases} \chi_{int} & \forall x : \phi(x) \leq 0 \\ \chi_{ext} & \forall x : \phi(x) > 0 \end{cases} \tag{34}$$

   such that for $\chi = \chi_{int}$, $s_{cal} = s$.

2. The level set equation is to be solved as follows

$$\frac{\partial \phi}{\partial t} + \nabla \phi \frac{\partial x}{\partial t} = 0 \tag{35}$$

3. As can be seen from 65, it is assumed that every point on the boundary moves perpendicular to the surface with some magnitude V (which will assume definition later in the process), such that

$$\frac{\partial x}{\partial t} = V(x,t).\frac{\nabla \phi}{|\nabla \phi|} \tag{36}$$

   So, on the boundary, 35 takes the form

$$\frac{\partial \chi}{\partial t} = (\chi_{int} - \chi_{ext})V(x,t) \tag{37}$$

4. As evolution begins, boundary of the domain (and consequently the domain) changes as $\delta D(t) = \{x : \phi(x,t) = 0\}$

5. Let $\mathcal{A}$ be the mapping from the forward model to the data. Then the cost function can be defined as

$$\mathrm{J}(\chi) = ||\mathcal{A}(\chi) - g||_2^2 \tag{38}$$

   Thus, the derivative of the cost function becomes

$$\frac{\partial J}{\partial t} =< \frac{\partial \mathcal{A}}{\partial \chi}.(\mathcal{A}(\chi) - g), \frac{\partial x}{\partial t} > \tag{39}$$

6. Thus, from 37 and 39, we can write the rate of change of cost function as,

$$\frac{\partial \mathrm{J}}{\partial t} = \int_{\delta D} (\chi_{int} - \chi_{ext}) V(x) \{ \frac{\partial \mathcal{A}}{\partial \chi} . (\mathcal{A}(\chi) - \mathcal{g}) \} \tag{40}$$

Thus, to ensure convergence of the procedure, a possible definition of V(x,t) could be,

$$V(x,t) = -\frac{\partial \mathcal{A}}{\partial t} (\mathcal{A}(\chi) - \mathcal{g})|_{\delta D(t)} \tag{41}$$

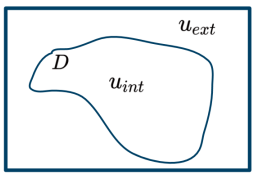

Figure 64: Domain of interest

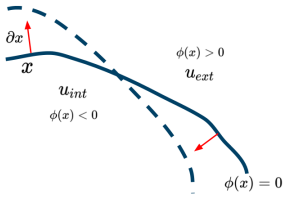

Figure 65: Variation of contrast with level set function at first iteration of level set

The implementation of the procedure outlined above has two drawbacks.

1. The entire procedure works only if $|\nabla\phi| = 1$ or, implicitly, if $\phi(x)$ is maintained as a signed distance function from the evolving boundary at all times.

2. All the expressions above have been defined for only the points at boundary.

Therefore, to alleviate these drawbacks, the implementation adopts a few special techniques namely evolving on the narrow band as in [14], extension of quantities (from a point where they're defined to points where they're not mathematically defined) as in [15] and reinitialization of ϕ as a signed distance function. As in [16], it can be casted as a regularization term in the expression for velocity in 41.
So, the potential function, $R_p(\phi) = \int p(|\nabla\phi|)dx$, is such chosen that $|\nabla\phi| = 1$ is maintained, where $p(s) = \begin{cases} \frac{1}{2}(s-1)^2 & \text{if } s \leq 1 \\ \frac{1}{(2\pi)^2}(1 - cos(2\pi s)) & \text{if } s > 1 \end{cases}$ Following the argument that led to 41, the complete expression for velocity of the points on the boundary can be given as

$$\frac{\partial \phi}{\partial t} = -\frac{\partial J}{\partial \phi} - \frac{\partial R_p(\phi)}{\partial \phi} = \mu . \nabla (\frac{p'(|\nabla\phi|)}{|\nabla\phi|} \nabla\phi) - \beta \mathrm{Re}\{(G_s D_v)'(G_s D_v \chi - s_v)\}(\chi_{int} - \chi_{ext}) \tag{42}$$

As this velocity is defined only on the boundary, extending V off the surface of ϕ should be such that $\nabla F . \nabla\phi = 0$ in order to ensure that ϕ remains a signed distance function. Following [14], V is allowed to be constant along normal to $\phi(t)$. Mathematically, V must satisfy

$$\frac{\partial V}{\partial t} + S(\phi) \frac{\nabla\phi}{|\nabla\phi|} \nabla V = 0 \tag{43}$$

where $S(\phi) = \begin{cases} -1 & \text{if } \phi < 0 \\ 0 & \text{if } \phi = 0 \\ +1 & \text{if } \phi > 1 \end{cases}$

The final algorithm is presented below. For numerical approximation, as in [5], central difference scheme is adopted for approximating spatial derivatives and forward difference scheme for temporal derivatives.

Algorithm 4 Born approximation using level-set evolution

Initialize $\chi = 0$ and $d_v = e_v$
while not convergence **do**
    Update gradient of cost function using 18
    procedure LEVEL SET EVOLUTION(Gradient, Initial ϕ)
        Initialise

$$\phi_0 = \begin{cases} 0 & \text{if (boundary pixel)} \\ -1 \times (\text{distance from the boundary}) & \text{otherwise} \end{cases} \tag{44}$$

        while not convergence **do**
            Calculate velocity according to 42 $\forall x : \phi(x) = 0$
            Define a narrow tube, $T = \{x : \phi(x) < \gamma\}$
            Extend velocity from step 2 $\forall x \in T$ using 43
            Fix values of ϕ at the inner and outer boundary of T
            Update the value of ϕ $\forall x \in T$ using 42 and the value calculated in step 4
            Assign the value of contrast as $\chi = \begin{cases} = \chi_{int} \text{ if } \phi \leq 0 \\ = \chi_{ext} \text{ if } \phi > 0 \end{cases}$
            Update J using 22
            if J<tolerance **then**
                Convergence = 1
            else
                Convergence = 0
    Update d_v using [7]
    Update J using 22
    if J<tolerance **then**
        Convergence = 1
    else
        Convergence = 0

7.7 Results

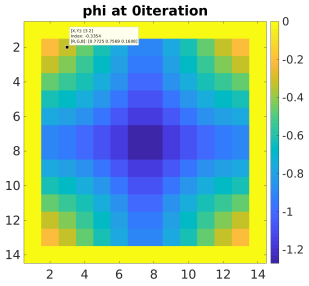

Figure 66: Initial level set function

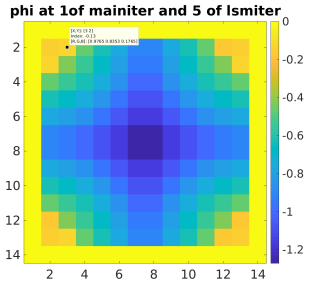

Figure 67: Level set function after 5 iterations of level set

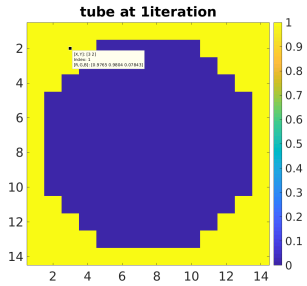

Figure 68: Narrow tube at first level set iteration

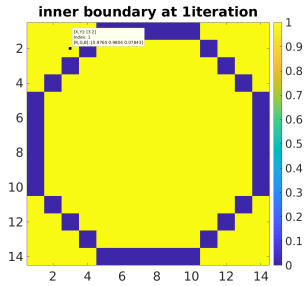

Figure 69: Inner boundary of the said tube

8 Conclusion and future work

As can be seen from 66 and 67, the level set algorithm works but still needs to be perfected as the shape of the boundary needs to change over iterations. Secondly, the method needs to be extended to more than scatterers. Further, the scatterers need to be modelled using sigmoid function instead of unit step function as it has been shown to give a higher convergence rate. Besides, the information exploited by detecting the edge on the gradient picture needs to be casted in the form of a regularizing term and convergence is to be shown mathematically. Finally, a hybrid of multimaterial level set using sigmoid and subspace optimization technique is expected to have a superior throughput in terms of computational cost as well as an accurate reconstruction.

References

[1] Y. M. Wang and W. C. Chew, "An iterative solution of the two – dimensional electromagnetic inverse scattering problem," *International Journal of Imaging Systems and Technology*, vol. 1, no. 1, pp. 100 – 108, 1989.

[2] ——, "Reconstruction of two-dimensional permittivity distribution using the distorted born iterative method," *IEEE Transactions on Medical Imaging*, vol. 9, no. 2, pp. 218 – 225, 1990.

[3] X. Chen, "Subspace-based optimization method for solving inverse-scattering problems," *IEEE Transactions on Geoscience and Remote Sensing*, vol. 48, no. 1, pp. 42 – 49, 2010.

[4] J. A. Sethian, "Evolution, implementation, and application of level set and fast marching methods for advancing fronts," *Journal of Computational Physics*, vol. 169, no. 2, pp. 503 – 555, 2001.

[5] P. Shah and M. Moghaddam, "A fast level set method for multimaterial recovery in microwave imaging," *IEEE Transactions on Antennas and Propagation*, vol. 66, no. 6, pp. 3017 – 3026, 2018.

[6] D. Shur, K. Yaswanth, and U. K. Khankhoje, "Two dimensional microwave imaging using a divide and unite algorithm," *2017 Progress in Electromagnetics Research Symposium - Fall (PIERS - FALL)*, pp. 1501 – 1508, 2017.

[7] J.Richmond, "Scattering by a dielectric cylinder of arbitrary cross section shape," *IEEE Transactions on Antennas and Propagation*, vol. 13, no. 3, pp. 334 – 341, 1965.

[8] K. Yaswanth, S. Bhattacharya, and U. K. Khankhoje, "Algebraic reconstruction techniques for inverse imaging," *2016 International Conference on Electromagnetics in Advanced Applications (ICEAA)*, pp. 756–759, 2016.

[9] E.Avots, H.S.Arslan, L.Valgma, J.Gorbova, and G.Anbarjafari, "A new kernel development algorithm for edge detection using singular value ratios," *Signal, Image and Video Processing*, vol. 12, no. 7, pp. 1301 – 1309, 2018.

[10] A.Banharnsakun, "Artificial bee colony algorithm for enhancing image edge detection," *Evolving Systems*, pp. 1 – 9, 2018.

[11] N. Kyurkchiev and S. Markov, "On the hausdorff distance between the heaviside step function and verhulst logistic function," *Journal of Mathematical Chemistry*, vol. 54, no. 1, pp. 109 – 119, 2016.

[12] ——, "Sigmoidal functions: some computational and modelling aspects," *Biomath Communications*, vol. 1, no. 2, 2014.

[13] F. Santosa, "A level-set approach for inverse problems involving obstacles," *ESAIM: Control, Optimisation and Calculus of Variations*, vol. 1, pp. 17 – 33, 1996.

[14] D. Peng, B. Merriman, S. Osher, H. Zhao, and M. Kang, "A pde-based fast local level set method," *Journal of Computational Physics*, vol. 155, no. 2, pp. 410 – 438, 1999.

[15] J. A. Sethian, "Evolution, implementation, and application of level set and fast marching methods for advancing fronts," *Journal of Computational Physics*, vol. 169, pp. 503 – 555, 2001.

[16] C.Li, C.Xu, C.Gui, and M.D.Fox, "Distance regularized level set evolution and its application to image segmentation," *IEEE Transactions on Image Processing*, vol. 19, no. 12, pp. 3243 – 3254, 2010.